REPORT DOCUMENTATION PAGE

Form Approved
OMB No. 0704-0188

1. REPORT DATE *(DD-MM-YYYY)*	2. REPORT TYPE	3. DATES COVERED *(From - To)*
9/30/2015	Final Report	10/23/12-9/30/15

4. TITLE AND SUBTITLE
Low-Absorption Liquid Crystals for Infrared Beam Steering

5a. CONTRACT NUMBER

5b. GRANT NUMBER
N00014-13-1-0096

5c. PROGRAM ELEMENT NUMBER

6. AUTHOR(S)
Dr. Shin-Tson Wu

5d. PROJECT NUMBER

5e. TASK NUMBER

5f. WORK UNIT NUMBER

7. PERFORMING ORGANIZATION NAME(S) AND ADDRESS(ES)
University of Central Florida
12201 Research Parkway, suite 501
Orlando, FL 32826-3246

8. PERFORMING ORGANIZATION REPORT NUMBER

9. SPONSORING/MONITORING AGENCY NAME(S) AND ADDRESS(ES)
Office of Naval Research
875 North Randolph Street
Arlington, VA 22203-1995

10. SPONSOR/MONITOR'S ACRONYM(S)
ONR 312

11. SPONSOR/MONITOR'S REPORT NUMBER(S)

12. DISTRIBUTION/AVAILABILITY STATEMENT
Approved for Public Release; Distribution is Unlimited

13. SUPPLEMENTARY NOTES

14. ABSTRACT

The objective of this project is to develop high birefringence, large dielectric anisotropy, and low optical loss nematic liquid crystals for infrared laser beam steering applications. To suppress the optical loss in MWIR and LWIR, we have investigated following approaches: (1) Employing a thin cell gap; (2) Red-shifting the absorption bands to outside the spectral region of interest by deuteration, fluorination, or chlorination; (3) Reducing the overtone absorption by using a short alkyl chain. We have synthesized several fluorinated and chlorinated terphenyl compounds and formulated a eutectic mixture showing high birefringence and low absorption (over 98% transmittance) in the MWIR region, while possessing a modest positive dielectric anisotropy and wide nematic range. To achieve fast response time, we developed a polymer network liquid crystal with 2-pi phase change at MWIR and response time less than 4ms. To extend the potential applications into LWIR, we synthesized several chlorinated terphenyl compounds with high birefringence and an aromatic ring-deuterated cyano-biphenyl compound to achieve high transmittance.

15. SUBJECT TERMS
Low absorption, deuterated, fluorinated and chlorinated liquid crystals, eutectic mixture, MWIR and LWIR spatial light modulators.

16. SECURITY CLASSIFICATION OF:			17. LIMITATION OF ABSTRACT	18. NUMBER OF PAGES	19a. NAME OF RESPONSIBLE PERSON
a. REPORT	b. ABSTRACT	c. THIS PAGE		39	Vicky Ortiz
					19b. TELEPHONE NUMBER *(Include area code)* 407-823-6825

ONR Final Report

Low-absorption liquid crystals for infrared beam steering

UCF Account Number: 6501-6248
ONR contract #: N00014-13-1-0096

Prepared for:	ONR Program Manager Dr. Peter Criag Email: peter.craig@navy.mil
Contract Period:	Oct. 23, 2012 to Sep. 30, 2015
Performance Period:	Oct. 23, 2012 to Sep. 30, 2015
Principal Investigator:	Prof. Shin-Tson Wu College of Optics and Photonics University of Central Florida Orlando, Florida 32816-2700 Email: swu@ucf.edu Tel: 407-823-4763 Fax: 407-823-6880

Abstract:

The objective of this project is to develop high birefringence, large dielectric anisotropy, and low optical loss nematic liquid crystals for infrared laser beam steering applications. To suppress the optical loss in MWIR and LWIR, we have investigated following approaches: (1) Employing a thin cell gap; (2) Shifting the absorption bands to outside the spectral region of interest by deuteration, fluorination, or chlorination; (3) Reducing the overtone absorption by using a short alkyl chain. We have synthesized several fluorinated and chlorinated terphenyl compounds and formulated a eutectic mixture showing high birefringence and low absorption (over 98% transmittance) in the MWIR region, while possessing a modest positive dielectric anisotropy and wide nematic range. To achieve fast response time, we developed a polymer network liquid crystal with 2π phase change at MWIR and response time less than 4ms. To extend the potential applications into LWIR, we synthesized several chlorinated terphenyl compounds with high birefringence and a phenyl ring-deuterated cyano-biphenyl compound to achieve high transmittance.

Key words: Low absorption, deuterated, fluorinated and chlorinated liquid crystals, eutectic mixture, MWIR and LWIR spatial light modulators.

1. Objective

The main objective of this program is to develop low-loss liquid crystals for electronic laser beam steering in the infrared region, especially for MWIR. Ideally, a single collimated beam of emissions from multiple lasers covering this broad band would be directed as a single beam with a common beam director. The major advantages of such a non-mechanical beam steering device are threefold: 1) reduction of system size-weight-and-power, 2) increasing mean-time-between-failure, and 3) reducing system complexity.

Beam steering based on liquid crystal (LC) optical phase array (OPA) has been demonstrated by Raytheon and Hughes since the 1980s. OPA has micro-radian precision, high diffraction efficiency and negligible side lobes, but its scanning angle is limited. To widen steering angle, one coarse OPA and one fine OPA are cascaded. For two-dimensional beam steering, two OPAs arranged in orthogonal directions are commonly configured.

Recently, Vescent Photonics developed a new *refractive* beam steering device using a LC layer as cladding in a slab waveguide. The evanescent field of the fundamental waveguide mode interacts with the LC layer near the surface of the waveguide where the LC molecules are well-ordered (low loss) and experience high restoring forces (<0.5 ms response time) and large steering angle. The major challenge of Vescent's beam steering device (SEEOR) is its relatively long optical beam path. In the visible and near IR spectral regions, most LCs have negligible absorption so that the optical loss is minimal. In the MWIR and LWIR regions, some closely overlapped molecular vibration bands exist. As a result, the baseline absorption coefficient of 5CB reaches 10/cm. In a 2π-modulo OPA, the employed LC layer is usually thinner than 10 μm. Thus, the absorption loss is ~1%. But in Vescent's SEEOR, the optical path length could range from 1 mm to 10 mm and the absorption loss could be significant. Thus, there is an urgent need to develop low-loss liquid crystals in order to extend SEEOR operation to MWIR and LWIR.

2. Technical Approach

A major challenge for IR applications of an LC device is the inherently large absorption loss due to some overlapping molecular vibration bands and their overtones. In the off-resonance regions, the baseline absorption coefficient of 5CB (cyano-biphenyl) reaches as high as α~10/cm [ST Wu, J. Appl. Phys. 84, 4462 (1998)]. The transmittance (T) of an LC layer can be expressed as

$$T = e^{-\alpha d}, \tag{1}$$

where α is the absorption coefficient and d is the LC layer thickness. Let us take α~10/cm as an example. For a 10-μm-thick LC layer, $\alpha d=0.01$ and the transmittance remains 99%. However, if the LC layer thickness (or effective optical path length) increases, then the absorption will increase exponentially, as Eq. (1) indicates. To improve transmittance, two approaches are commonly pursued: 1) To minimize absorption coefficient α by selecting proper functional groups, while maintaining nematic phase; 2) To reduce the cell gap d or optical path length by using a high birefringence LC material. Here we define a figure-of-merit (*FoM*) to compare the performance of an LC:

$$FoM = \frac{\Delta n}{\alpha}. \tag{2}$$

The molecular vibration frequency (ω) of a diatomic group depends on the spring constant (κ) and the effective mass (m) as:

$$\omega = \sqrt{\kappa/m}. \quad (3)$$

As the effective mass increases the vibration frequency decreases, i.e., the absorption band shifts toward a longer wavelength. Table 1 shows some common absorption bands that occur in MWIR and LWIR regions: e.g., CH stretching, CN stretching, C=C stretching in phenyl rings, C-H in-plane deformation, C-C skeletal stretching, C-F stretching, and C-H out-of-plane deformation.

Table 1: IR absorption of different functional groups in typical liquid crystals. (str.=stretching; s.=strong absorption; m.=medium absorption; def.=deformation; w.=weak absorption; v.=variable intensity) [B. D. Mistry, *A Handbook of Spectroscopic Data: Chemistry-UV, IR, PMR, CNMR and Mass Spectroscopy,* Oxford, 2009]

	Vibration mode	Frequency (cm^{-1})	Wavelength (μm)	Relative intensity
C-H in phenyl ring	str.	3095-3010	3.23-3.32	m.
$-CH_2-$, $-CH_3$	str.	2950-2845	3.39-3.51	m.
C≡N	str.	2185-2120	4.58-4.72	s.
C≡C (non terminal)	str.	2260-2190	4.42-4.57	very weak
C-H in phenyl ring	str. overtone	1850-1780	5.40-5.62	m.
C=C	str.	1625	6.16	v.
C-H in $-CH_2-$	def.	1485-1445	6.74-6.92	m.
C-H in $-CH_3$	def.	1470-1430	6.80-7.00	m.
C-H in phenyl ring	in-plane def.	1225-950	8.16-10.53	w.
C-C	skeletal str.	1300-700	7.69-14.29	m.
C-F	str.	1100-1000	9.01-10.00	s.
$-CF_2-$	str.	1250-1050	8.00-9.50	s.
$-CF_3$	str.	1400-1100	7.14-9.10	s.
C-Cl	str.	800-600	12.5-16.67	s.
C-H in phenyl ring	out-of-plane def.	900-670	11.11-14.93	w.

More specifically, in the MWIR region the following absorption bonds dominate: the C-H stretching in a phenyl ring,–CH_2– and –CH_3 stretching from an alkyl chain, C≡N stretching from the cyano polar group, and some overtones from in-plane and out-of-plane C-H deformations. On the other hand, in the LWIR region following absorption bands dominate: C-H in-plane and out-of-plane stretching, C-C skeletal stretching, and C-F stretching.

From Eq. (3), three approaches can be considered to shift the absorption bands outside the spectral region of interest: deuteration, fluorination, and chlorination.

1) Deuteration: Substituting hydrogen with deuterium doubles the effective mass. As a result, the molecular vibration frequency would shift toward a longer wavelength by a factor of $\sqrt{2}$. The

C-D in-plane and out-of-plane deformations would occur outside the LWIR region. However, deuteration shifts the C-H vibration in alkyl chain (~3.5 μm) to ~4.8 μm [ST Wu, et al. J. Appl. Phys. 92, 7146 (2002)]. *Therefore, to reduce absorption for both LWIR and MWIR bands we should do deuteration only for the phenyl rings, but not for the alkyl chain.*

2) Fluorination: As shown in Table 1, the vibration frequencies of CF, CF_2 and CF_3 occur in the LWIR region. *Therefore, fluorination could be favorable for MWIR but is unfavorable for LWIR.* However, a special caution must be taken. From Table 1, the overtones of CF, CF_2 and CF_3 could appear in the MWIR region. This is indeed observed in our recent studies of fluorinated terphenyl liquid crystal in the MWIR region [Y. Chen, et al. Opt. Express 19, 10843 (2011)]. Although the overtone intensity is reduced significantly, it is still noticeable especially when the optical path length is long.
3) Chlorination: As shown in Table 1, the C-Cl vibration frequency occurs at 800-600 cm^{-1}, which is outside the LWIR band. Moreover, its overtone will not show up in the MWIR region. Therefore, from an absorption viewpoint C-Cl seems to be a better polar group than CN and CF. We have previous experiences in chlorinated liquid crystals [ST Wu, et al. Liq. Cryst. 10, 635 (1991)], but not aimed for IR applications. Here we report some new chloro LC compounds with special emphasis on low IR absorption.

On the other hand, a high birefringence LC is considered to reduce the cell gap d or optical path length. Thinner cell gap also helps to achieve fast response time for nematic liquid crystal. The LC birefringence is governed primarily by the molecular conjugation, which is contributed by the core structure and terminal groups. Due to UV instability of double bonds and carbon-carbon triple bonds, conjugated phenyl rings have been commonly used for obtaining high birefringence. However, using too many phenyl rings will result in several drawbacks: 1) its melting point will be too high to be used at room temperature; 2) its viscosity will increase; 3) its birefringence will saturated once there are more than four phenyl rings. Therefore, terphenyl could be an optimal core structure. In terms of polar group, -F,-Cl,-NCS, -CN are commonly used in LC compounds to provide dipole moment. With the same core structure, -F and –Cl provide large resistivity and modest dipole moment. Therefore, they are widely used in the TFT-LCDs. –NCS provides large birefringence and dielectric anisotropy with keeping modest viscosity, while its properties will deteriorate after UV exposure. –CN helps increase birefringence, dielectric anisotropy and shows good UV stability, while it may result in large viscosity and response time. To achieve fast response time, polymer network liquid crystal (PNLC) is considered.

3. Accomplishments

3.1 Benchmark: 5CB

In our study, liquid crystal 5CB is used as benchmark, whose chemical structure is shown in the inset of Fig. 1. We measured the absorption coefficient of 5CB (in an isotropic phase) using FTIR (Spectrum Two, Perkin Elmer).

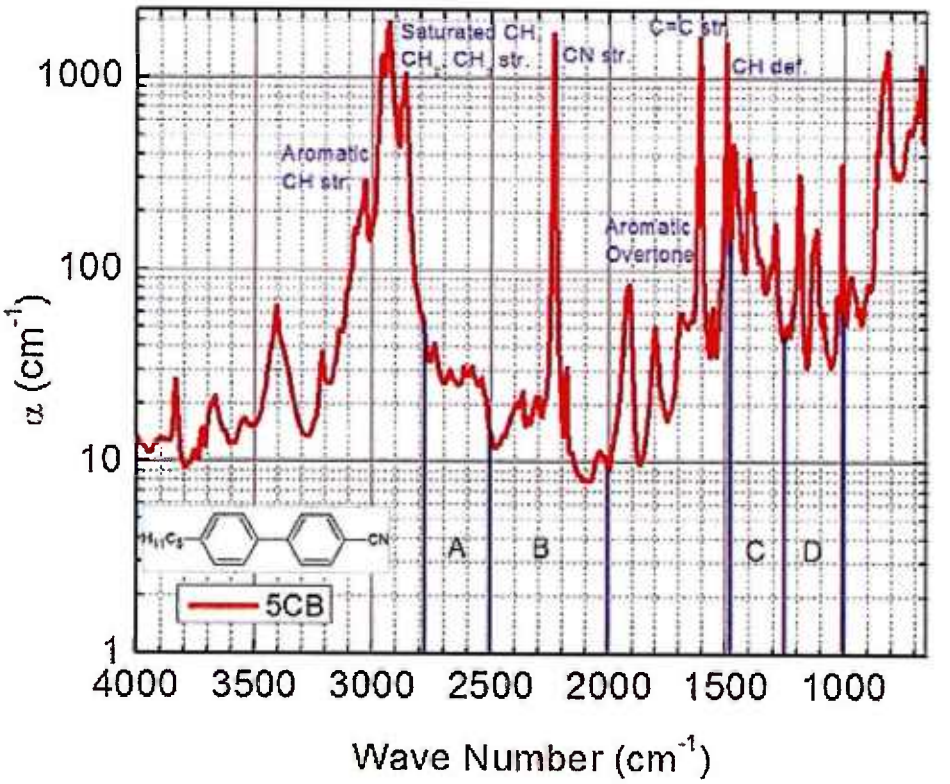

Fig. 1. Measured absorption coefficient of 5CB.

Figure 1 depicts the measured absorption coefficient of 5CB from 4000 cm^{-1} to 650 cm^{-1}. The C-H stretching band (including $-CH_2$ and $-CH_3$) is quite broad (3300-2800 cm^{-1}) and strong, and the peak absorption coefficient exceeds 600 cm^{-1}. In the center of MWIR (2500 cm^{-1} to 2000 cm^{-1}, marked as Zone B in Fig. 1), the C≡N stretching shows a narrow but very strong absorption (α>1000 cm^{-1}). Cyano is a strong polar group, which not only provides a large dielectric anisotropy but also extends the conjugation length for enhancing birefringence. For practical applications, a large $\Delta\varepsilon$ helps to reduce operation voltage while high Δn enables a thinner LC layer to be used for reaching the required phase change. Unfortunately, C≡N has a strong absorption at λ=4.45 μm and should be avoided because it will lift up the baseline absorption. A molecular vibration band usually has Lorentzian shape and its tail could spread broadly. The overlap of the neighboring bands is responsible for the observed baseline absorption.

Besides the normal vibration mode of C≡N, the baseline absorption in Zone B also comes from the overtone (doubled frequency) of the absorption bands in Zone D, as marked in Fig. 1. As listed in Table 2, the C-C (in the alkyl chain) skeletal stretching (1300-700 cm^{-1}) and the in-plane deformation of C-H in the phenyl rings (1225-950 cm^{-1}) contribute to the absorption in Zone D.

The absorption of Zone C consists of the -C-H (in alkyl chain) deformation and C-C skeletal stretching, whose overtone further increases the baseline absorption observed in Zone A. The tail of the absorption band in Zone A may also raise the absorption level in Zone B.

In summary, the absorption in MWIR (Zones A and B) are primarily influenced by the strong C≡N stretching and the overtone/combination absorption from Zones C and D.

Table 2. Possible absorption mechanisms for Zones A-D shown in Fig. 1.

Zone	Absorption mechanism	Frequency (cm^{-1})	Wavelength (μm)
A	C-H (in CH_2, CH_3) def. overtone C-C skeletal str. overtone	2790-2500	3.58-5
B	C≡N str. C-H (in phenyl ring) in-plane def. overtone C-C (in alkyl chain)skeletal str. overtone Combination	2000-2500	4-5
C	C-H in CH_2, CH_3 def. C-C skeletal str.	1485-1250	6.73-8
D	C-H (in phenyl ring) in-plane. def C-C (in alkyl chain)skeletal str.	1000-1250	8-10

3.2 Fundamental modes

3.2.1. Undesirable polar groups: C≡N and NCS

As shown in Sec. 3.1, C≡N has a strong absorption at λ=4.45 μm and should be avoided for broadband application. Besides C≡N group, NCS and C-F are two other commonly used polar groups. Compounds with different polar groups were prepared, dissolved in CCl_4 at a concentration of ~$5x10^{-5}$ mol/ml and then filled in a NaCl cell with cell gap (0.5 mm). The transmission spectra were measured using FTIR, as shown in Fig. 2. NCS exhibits a very strong and broad absorption from 2220-1923 cm^{-1}, while C-F has an absorption band (1100-1000 cm^{-1}), which is outside the MWIR spectral region [Table 1].

Another polar group C-Cl can also be employed since its absorption is in the range of 800-600 cm^{-1}, and its second harmonic overtone will not show up in Zone B.

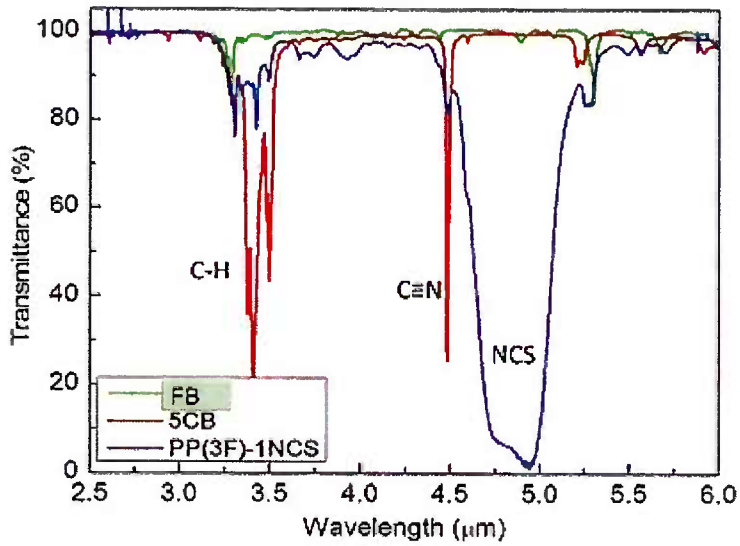

Fig. 2. Measured transmission spectra of three compounds with different polar groups. FB stands for F-Ph-Ph-F, where Ph is a phenyl ring.

3.2.2. Tolane

Tolane core is effective for elongating the conjugation length and enhancing birefringence. Theoretically, as a linking group C≡C exhibits a much weaker absorption than it is as a terminal group. We measured the absorption coefficient of a tolane compound PTP-20F, and results are depicted in Fig. 3. The absorption peak of C≡C occurs at 2216 cm^{-1} and its α is ~6X smaller than that of C≡N bond. However, this absorption peak raises the absorption baseline to >10cm^{-1} in the 2500-2000cm^{-1} region. Thus, C≡C is not a favorable linking group and should be avoided.

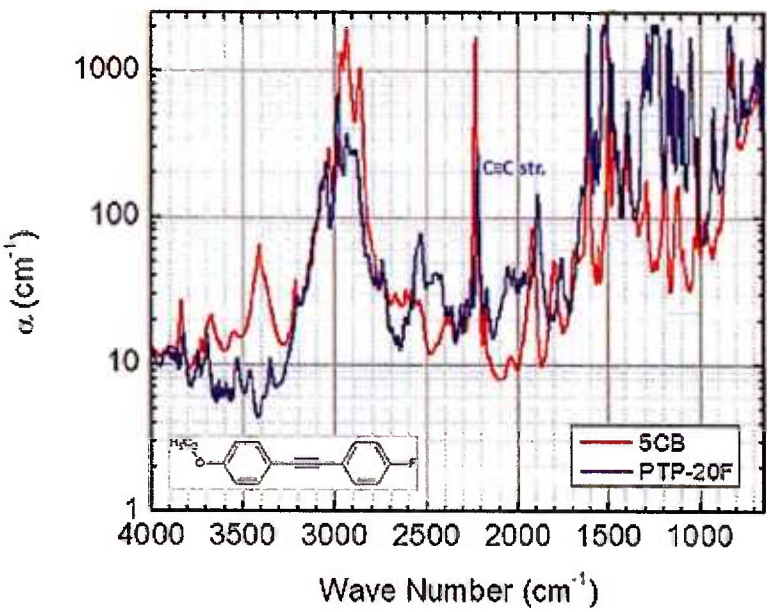

Fig. 3. Measured absorption coefficient of PTP-20F vs. 5CB.

3.3 Reducing overtone absorption

3.3.1. Avoiding C-O group

C-O group helps to stabilize mesongenic phase. The absorption of C-O group occurs at 1272-1200 cm^{-1}, but its overtone appears in 2540-2400 cm^{-1} [Fig. 3]. Therefore, we should avoid using C-O functional group.

3.3.2. Short alkyl chain

To study how alkyl chain affects the MWIR absorption, we measured the absorption coefficient of bi-phenyl compounds by FTIR. Figure 4 depicts the absorption spectrum of PP-2 and PP. The structures of PP-2 and PP are included in Fig. 4. Due to the absence of alkyl chain, PP shows lower absorption baseline in the whole IR region and the lowest absorption coefficient is less than 2 cm^{-1} at ~3500cm^{-1}. Both of them show a relatively strong resonance peak near 3000 cm^{-1}, which corresponds to the =C-H (in phenyl rings) stretching absorption. The absorption in 2950-2845 cm^{-1} comes from the –C-H (in alkyl chain) stretching absorption, which only occurs for PP-2. Besides that, PP also shows much lower overtone absorption in the spectrum region of interest 2500-2000 cm^{-1}. A shorter or even without alkyl chain will help reduce the absorption. But neither PP nor PP-2 has a LC phase. Flexible chain is favored to induce nematic phase. Thus, we need to compromise between the nematic phase and absorption when designing low-loss LCs.

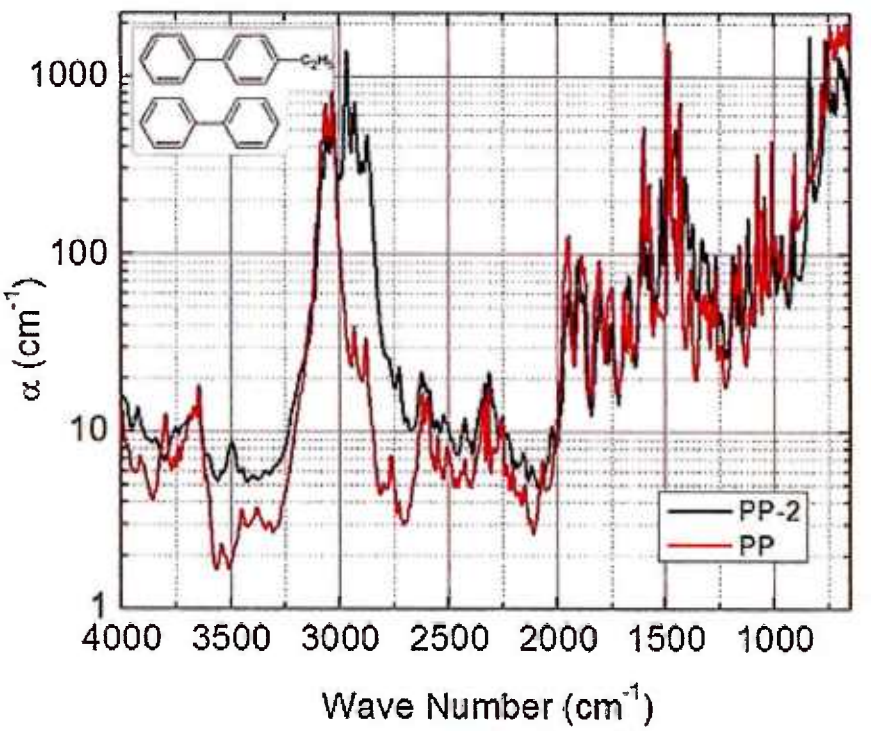

Fig. 4. Measured absorption coefficient of PP vs. PP-2.

Since the presence of alkyl tails results in larger absorption in the MWIR region, an extreme example is to eliminate all the alkyl chain, while keeping nematic phase. To ensure large aspect ratio for mesongenic phase, quaterphenyl compounds are investigated. As shown in Fig. 5, without any alkyl chain, the first compound shows enantiotropic nematic phase. The quaterphenyl

molecule without any substitution (the middle compound in Fig. 5) has high level of π-π interaction leading to efficient molecular packing. Such interaction results in high melting point [322 °C; Beilstein, J. Org. Chem. 9, 698–704 (2013)]. To lower the melting point and render the molecule useful for IR applications, disruption of the molecular packing is needed. Chlorine substitution can be used for reducing the ring coplanarity of the quaterphenyl molecule. By introducing one chlorine substitution, the melting point of the third compound drops 150 °C, compared to the second compound. The substitution position also matters in terms of the temperature range, and we will further study on this and find useful LC compound structures.

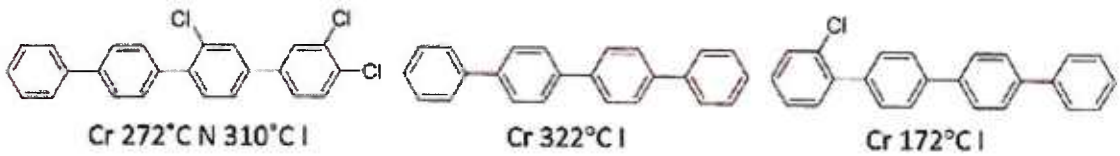

Fig. 5. Molecule structure and phase transition temperature of quaterphenyl compounds.

3.3.3. Reducing =C-H in-plane deformation absorption

Phenyl ring is a very common group in LCs since it helps to increase Δn and it's more stable compared to tolane. But the in-plane deformation of =C-H (1225-950 cm^{-1}) in the phenyl rings occurs and its overtone contributes to the absorption in 2500-2000 cm^{-1}. For comparison, we measured the absorption spectrum of a compound with no unsaturated bonds 5CC2. 5CC2 has sematic phase from -16 °C to 77 °C and its chemical structure is shown in Fig. 6.

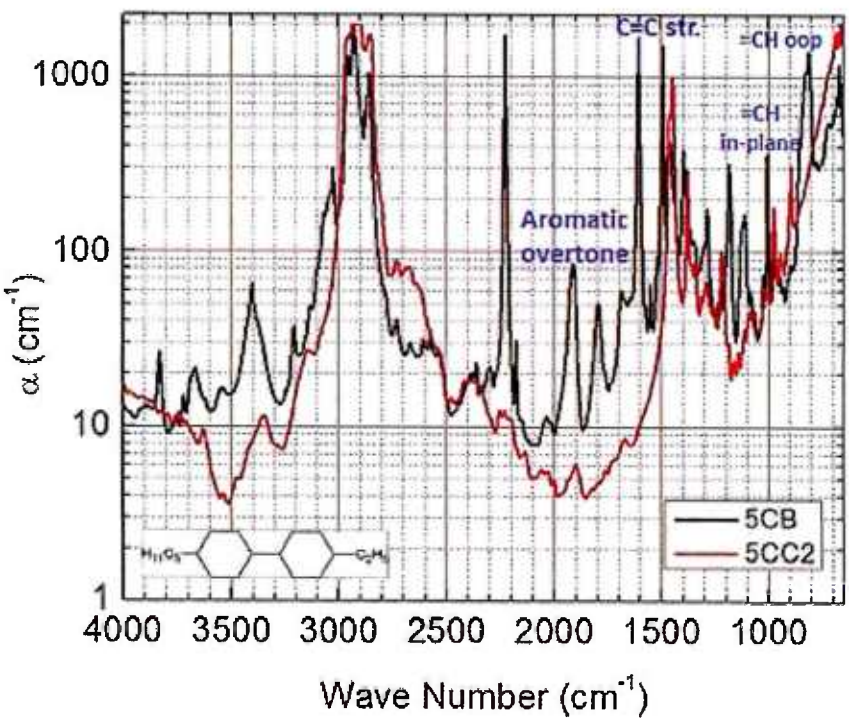

Fig. 6. Measured absorption coefficient of 5CC2 and 5CB.

From Fig. 6, the absorption of 5CC2 is very low from 2200-1700cm^{-1} due to the absence of

aromatic overtone. For application in this spectral region, we may consider to use the saturated compounds. However, the birefringence is relatively low (~0.05). On the other hand, this study proves that the overtone of =C-H deformation contributes significantly to the absorption in 2500-2000 cm^{-1}. Proper substitution in the phenyl rings with F or Cl can decrease the number of =C-H bonds and hence reduce the in-plane deformation absorption. We will discuss about the fluorination and chlorination in the following two sessions respectively.

3.3.4. Fluorination

If a hydrogen atom in the phenyl ring is substituted by fluorine, the corresponding =C-F deformation will shift toward a longer IR region. The fundamental absorption of C-F stretching occurs at 1229 cm^{-1} and 1159 cm^{-1}, which are out of MWIR range. However, the overtone of this stretching could also contribute to the absorption in the 2500-2000 cm^{-1}. To quantitatively study this effect, we measured the absorption spectra of PP-2 and 2PPF, whose chemical structures are shown in the inset of Fig. 7. They have the same core structure and alkyl chain length, except there is a fluorine atom at the end of the phenyl ring for 2PPF. From Fig. 7, there are two strong additional absorption bands showing up at 1229 and 1159 cm^{-1}. And the overtone raises the absorption coefficient of 2PPF in the 2500-2000 cm^{-1} region, although only one fluorine atom is introduced. Thus, fluorination is not a good choice for lowering the absorption in the MWIR region because of its overtone absorption.

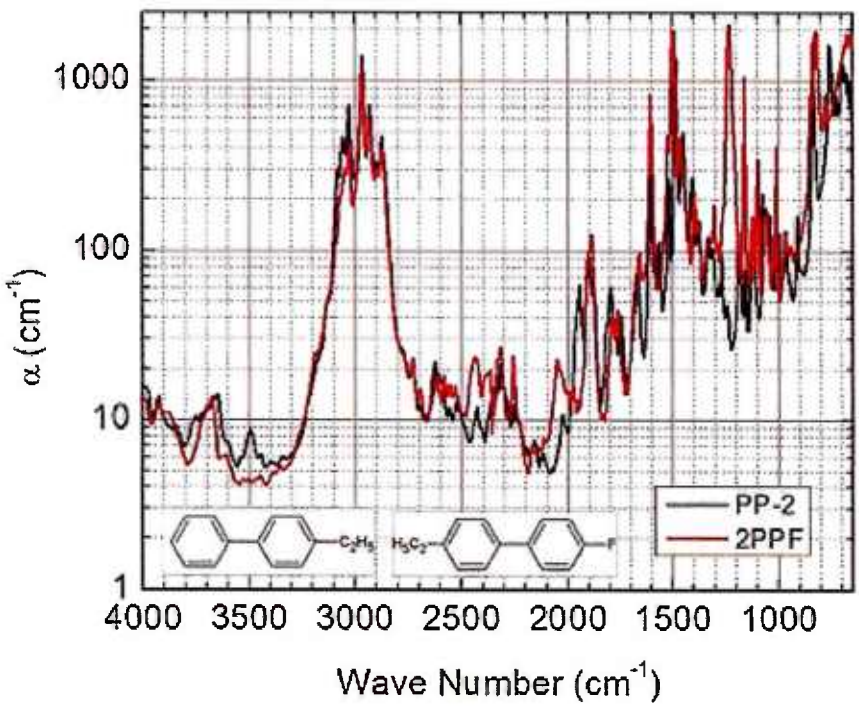

Fig. 7. Measured absorption coefficient of PP-2 vs. 2PPF.

However, the situation could change if we do complete fluorination in the alkyl chain because all the saturated –C-H bond stretching absorption at ~2900 cm^{-1} would shift to ~1100 cm^{-1} for the –C-F bond (stretching absorption). Thus, we could eliminate the strong and broad absorption in

the 3000 to 2600 cm^{-1} region. One tradeoff is that fluoride atom is much heavier than hydrogen atom, and may suppress the liquid crystal phase or increase the melting point significantly.

3.3.5. Chlorination

Besides fluorination, chlorination in the phenyl ring is another option to shift the =C-H in-plane deformation absorption to a longer wavelength. Based on Eq. (3), since chloride has even heavier atomic mass, the C-Cl stretching absorption occurs at 650 cm^{-1}, whose second harmonic absorption would locate outside of the 2500-2000 cm^{-1} region. Figure 8 shows the absorption spectrum of 2PPCl. The baseline of the 2PPCl is much lower than that of 5CB due to the shorter alkyl chain and the absence of CN group. The lowest absorption coefficient is ~4 cm^{-1} at ~2150 cm^{-1}. Thus, chlorination is an effective way to achieve low absorption in MWIR.

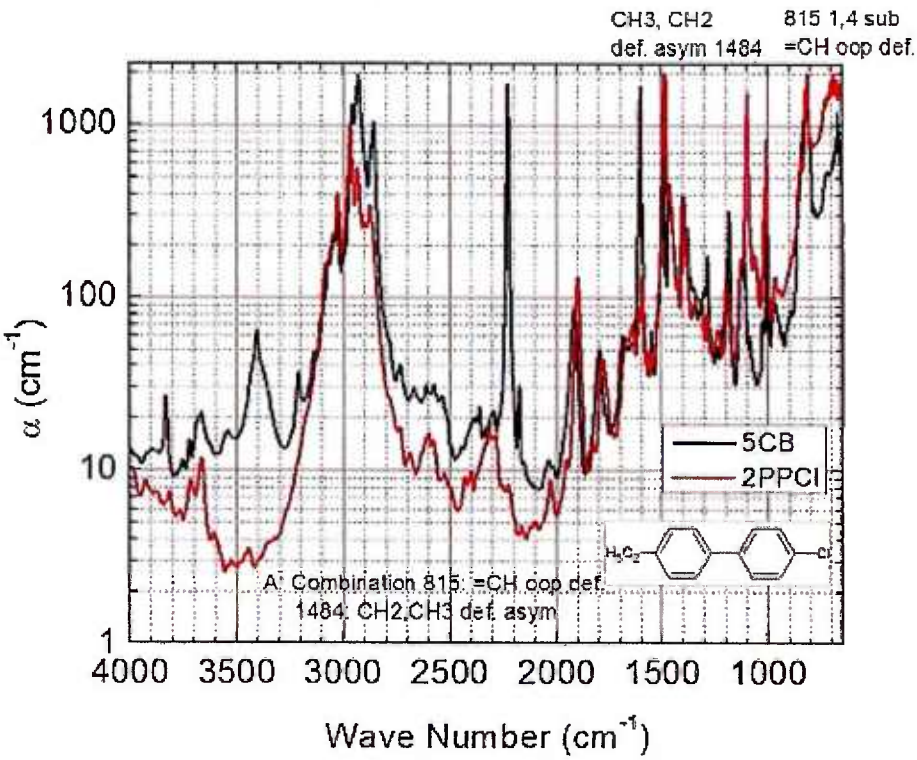

Fig. 8. Measured absorption coefficient of 5CB and 2PPCl.

3.3.6. Reducing combination absorption

From Fig. 8, we noticed that there is an unexpected absorption peak near 2300 cm^{-1}. It is not corresponding to any second harmonic absorption. We suspect that it might result from higher order overtone or combination absorption of lower frequency (sum frequency). $-CH_2$ and $-CH_3$ (in alkyl chain) asymmetric deformation occurs at ~1484 cm^{-1}, and =C-H (in phenyl ring) out-of-plane deformation contributes to the strong peak at ~815 cm^{-1}. The sum frequency of these two absorption bands is speculated to cause the absorption at ~2300 cm^{-1}. The combination absorption is difficult to predict, but the magnitude is much smaller compared to the fundamental absorption. But if the optical path is long (cm), this small absorption coefficient could still be quite significant.

3.4 Low absorption LC compounds and mixtures

Table 3. Chemical structures and properties of the eleven compounds studied, where Cr stands for crystalline, N for nematic, and I for isotropic Phase

No.	Structure	PTT(°C)
1	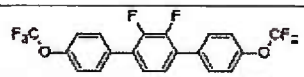	Cr 86 N 88 I
2	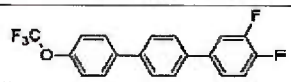	Cr 86 N (84) I[a]
3	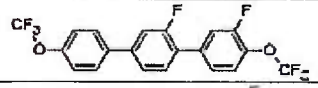	Cr 55 N (40) I
4	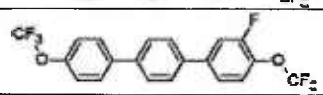	Cr 113 I
5	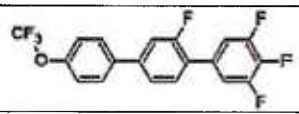	Cr 66 I
6	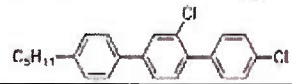	Cr 71 (N 65) I
7	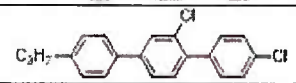	Cr 95 (N 68) I
8	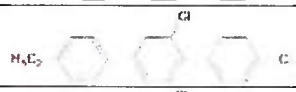	Cr106.29(N70.6)I
9		Cr78.3(N45)I
10	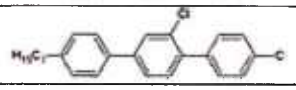	Cr72(N67)I
11	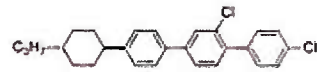	Cr 140 N 257 I
12	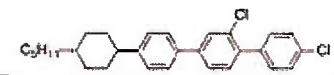	Cr 128 N 253 I
13	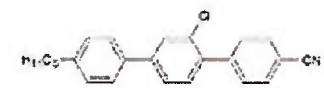	Cr 72 N 98 I

1. [a]() indicates a monotropic phase

Based on our design strategies, we prepared five fluoro and two chloro-terphenyl compounds as listed in Table 3. The synthesis processes will be discussed in Section 4. To suppress absorption, we replace all the CH bonds in the alkyl chain by $-OCF_3$, but keep the CH bonds in the phenyl rings in order to obtain nematic phase. Moreover, the CH bonds in the phenyl rings exhibit a much weaker and narrower absorption than those in the flexible alkyl chain. The phase transition temperatures (PPAs) were measured by Differential Scanning Calorimetry (DSC, TA instruments Q100). The first three compounds have nematic phase. To widen the nematic range, we formulated a eutectic mixture, designated as UCF-1, using these 5 fluoro compounds. The melting point (T_m)

is 42°C and clearing point (T_c) is 51.5°C during the heating process. The T_c drops to below –10°C due to super-cooling.

3.4.1 Low absorption

To measure MWIR absorption, we filled UCF-1 to a LC cell with two bare barium fluoride (BaF_2) substrates and measured their transmittance using a Perkin Elmer Spectrum One FTIR Spectrometer. BaF_2 is highly transparent from UV to ~10μm. It refractive index 1.47 is close to that of LC. The cell gap is ~46μm. To eliminate scattering, we conducted the absorption measurement at an isotropic phase (~60°C). To take surface reflections into consideration, we use a single BaF_2 as the reference. Figure 9 shows the measured absorption coefficient of UCF-1. Also included for comparison is 5CB. For UCF-1, it shows a relatively low absorption coefficient (α~2.3 cm^{-1}) in the vicinities of 3333 cm^{-1}, i.e. λ~3μm, and the absorption coefficient is smaller than 3 cm^{-1} in the region of 3571-3333 cm^{-1} (2.8~3.0 μm). Besides, the absorption at 3030-2778 cm^{-1} (3.3~3.6 μm) is significantly reduced because the alkyl chain has been replaced. The absorption peak at 3049 cm^{-1} (3.28 μm) originates from the CH vibration in the phenyl rings. It overlaps with the peak of 5CB very well. Even though the absorption peak resulting from C-O and C-F stretching vibrations are shifted to the 1302-1156 cm^{-1} (7.68~8.65μm), their combination overtone results in a modest (~80cm^{-1}) but broad absorption peak in the vicinities of λ=4 μm.

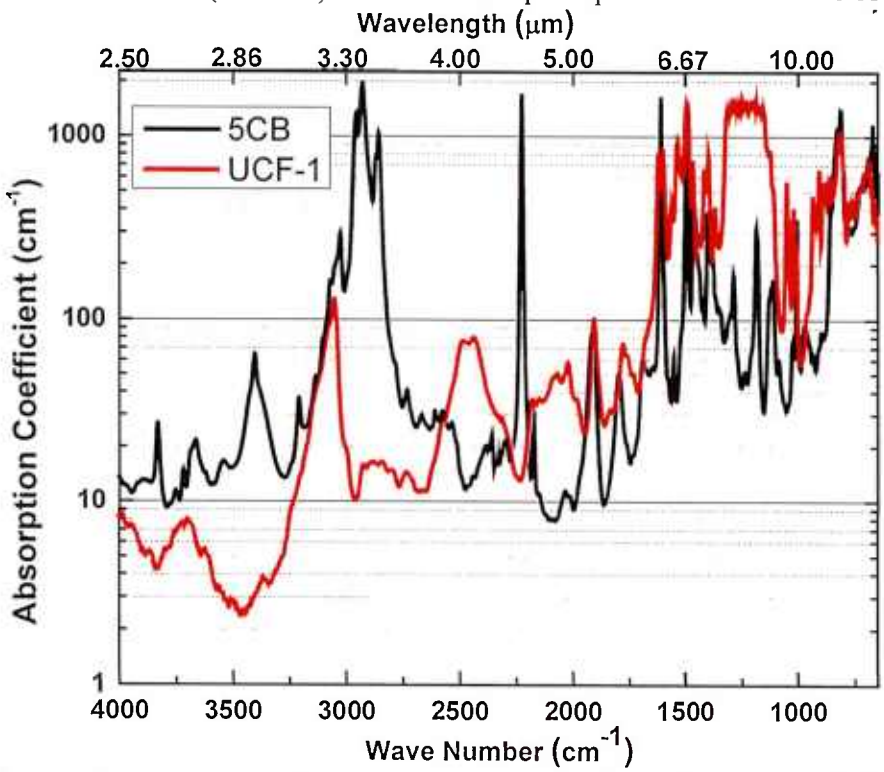

Fig. 9. Measured absorption coefficient spectrum of 5CB (black line) and UCF-1 (red line).

To shift overtone resonance peak out of MWIR, we replaced the fluorine with a heavier atom, chlorine. While, for chlorinated compounds, the alkyl chains need to be kept to maintain the flexibility and aspect ratio of the LC compounds. Otherwise, some undesirable properties, such as high melting point, large heat fusion enthalpy, and high viscosity could occur. More seriously, the compounds may not have any mesogenic phase. The physical properties of chlorinated LC for

display applications have been reviewed elsewhere. Thus, we synthesized two chlorinated compounds (#6 and #7) listed in Table 3. Both compounds exhibit monotropic phase. We prepared a binary mixture with 60 wt% compound 6 and 40 wt% compound 7, designated as UCF-2. The nematic range of UCF-2 is from 48.3°C to 69.2°C in the heating process. Super-cooling effect lowers the melting point to ~0°C. Thus, UCF-2 remains liquid crystal phase at room temperature (~25°C). To measure the MWIR absorption spectrum, we filled UCF-2 to a BaF_2 cell with cell gap ~46μm. The measurement procedures are the same as UCF-1.

Figure 10 depicts the measured absorption spectrum of UCF-2 in the IR region. The absorption spectrum of 5CB is also included for comparison. UCF-2 exhibits a relative clean absorption in the 4000-3125cm^{-1} (2.5~3.2μm). The lowest α is 4 cm^{-1} at 3247cm^{-1} (3.08μm), which is slightly higher than that of UCF-1. The responsible absorption mechanism in this region is the CH in-plane deformation. In UCF-1, more CH bonds are substituted by C-F bonds so that the in-plane vibration effect is suppressed.

More importantly, UCF-2 shows a relatively small absorption in 2778-1923 cm^{-1} (or 3.6μm to 5.2μm) window. The reasons are twofold: 1) In comparison with 5CB, the CN vibration band centered at 4.45μm is removed, and 2) In comparison with UCF-1, the vibration peaks resulting from C-Cl bonds are shifted to beyond 12.5 μm, and thus the overtone is still outside the MWIR region. The strong resonance peak centered at 2941cm^{-1} (3.4 μm) is due to the CH bonds at alkyl chain. Thus, it has similar shape to the resonance peak of 5CB but with weaker amplitude, because 5CB has a longer alkyl chain than the chlorinated compound (#7). Thus, UCF-2 shows a lower absorption than 5CB in the 4-5 μm MWIR region.

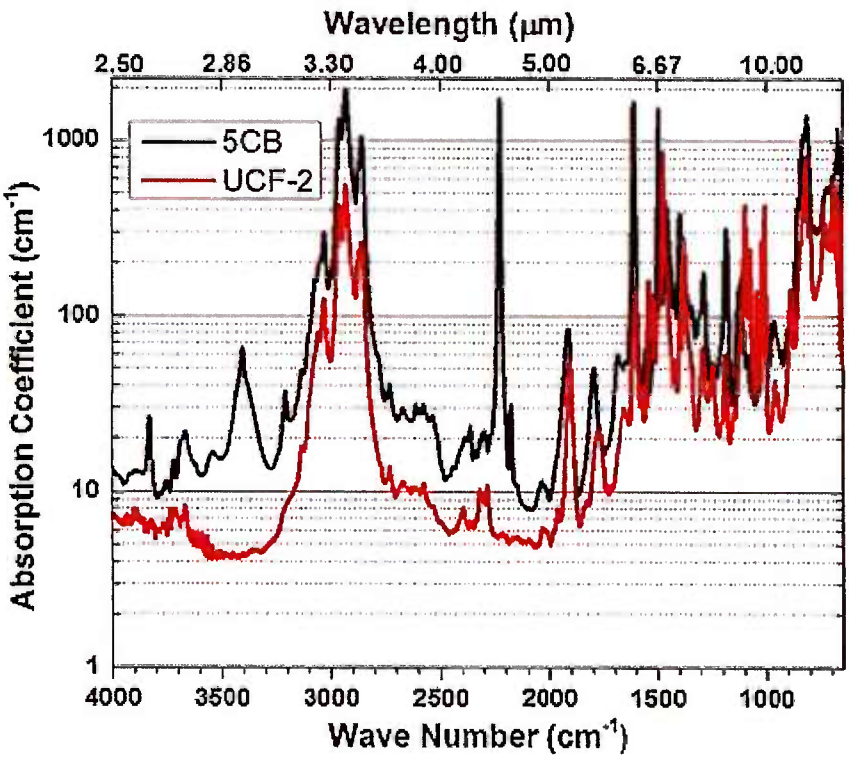

Fig. 10. Measured absorption coefficient of 5CB (black line) and UCF-2 (red line).

Table 3 also lists other chlorinated compounds we have synthesized (#8~#13). In all cases a *p*-

terphenyl core unit is employed to obtain high birefringence. To lower the melting point of UCF-2, we formulated a eutectic mixture (IR-M1) by adding #10 and it exhibits an enantiotropic phase with T_c=68°C. Compounds 11 and 12 are chlorinated cyclohexane terphenyls. Although their melting points are relatively high, their nematic temperature ranges are over 100°C. Therefore, to widen the nematic range, we doped 10 wt% of compound 12 into IR-M1 to give a new mixture designated as UCF-3. Compound 11 was not employed here because of its poor solubility, high melting point and large heat of fusion. Remarkably, the melting point of mixture UCF-3 drops to less than -40°C (limited by our DSC) and its clearing point is 85°C. We kept UCF-3 at –40°C for 3 hours and it did not crystalize. Thus, UCF-3 exhibits a wide nematic range including room temperature. Compound 13 is a chlorinated cyano-terphenyl. For the MWIR region, the cyano group should be avoided since it has a very strong absorption peak at ~4.48μm. However, the cyano group elongates the conjugation length and increases the birefringence, which helps to reduce the cell gap and improve the transmittance at LWIR region.

3.4.2 Physical properties evaluation

In addition to low absorption, the mixture is also required to have high birefringence, low viscosity and modest dielectric anisotropy. Therefore, we also characterized its physical properties.

A. Birefringence

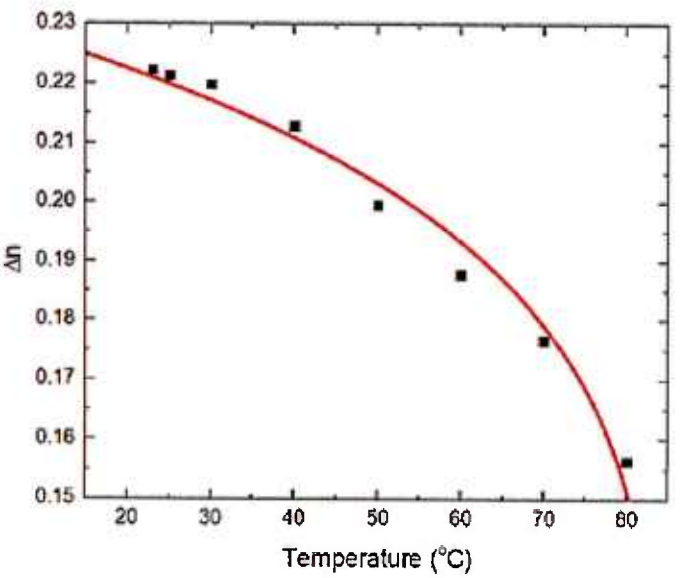

Fig.11. Temperature dependent birefringence of UCF-3 at λ=633nm: dots stand for measured data and red line for fitting curve with Eq. (5).

Birefringence can be obtained by measuring the voltage dependent transmittance of a homogeneous cell sandwiched between two crossed polarizers. We prepared two homogeneous cells with strong anchoring energy and cell gap d~5μm. In the visible and near IR regions, we can still use indium-tin-oxide (ITO) coated glass substrates. UCF-1 and UCF-3 were filled into the LC cells at ~70°C and 80°C, respectively. Then, both cells were mounted on a Linkam LTS 350 Large Area Heating/ Freezing Stage controlled by TMS94 Temperature Programmer. To obtain maximum transmittance, the LC director was oriented at 45° with respect to the polarizer

transmission axis. A linearly polarized He-Ne laser (λ=633nm), a tunable Argon-ion laser (λ=514nm, 488nm and 457nm) and a semiconductor laser (λ=1550nm) were used as the light sources. A 1 kHz square-wave AC signal was applied to the LC cells. The transmitted light was measured by a photodiode detector and recorded by a LabVIEW data acquisition system (DAQ, PCI6110). Thus, the corresponding VT curves and phase retardation were measured. The birefringence at a given wavelength and temperature was obtained from the phase retardation based on the following equation:

$$\delta = 2\pi d\Delta n / \lambda, \tag{4}$$

here, δ is the phase change, d is the cell gap, Δn is the birefringence and λ is the operation wavelength.

The temperature dependent birefringence for UCF-3 was measured from 20°C to 80°C, and the results for λ=633nm are plotted in Fig. 11, where dots are experimental data and red line is the fitting curve based on Haller's semi-empirical equation:

$$\Delta n = \Delta n_0 (1 - T/T_c)^{\beta}, \tag{5}$$

here Δn_0 is the extrapolated birefringence at T=0K and β is a material constant. Through fitting, we find $\Delta n_0 = 0.29$ *and* $\beta = 0.15$.

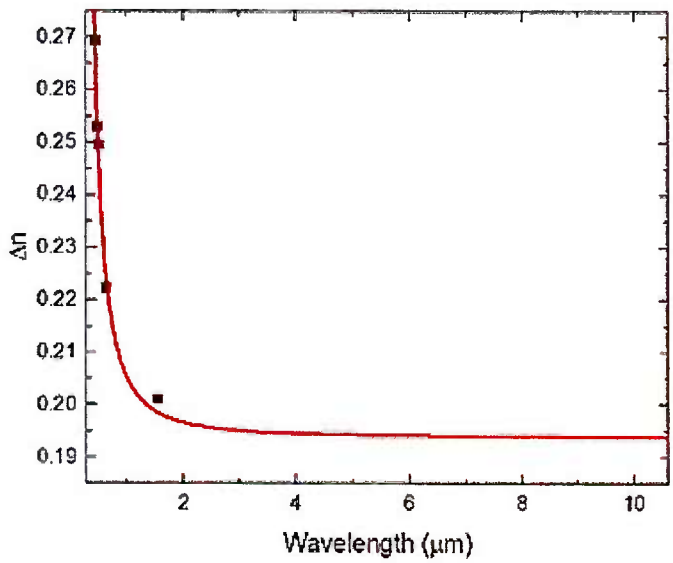

Fig. 12. Birefringence dispersion of UCF-3 at room temperature: dots are measured data and solid line is fitting with Eq. (6).

To determine the birefringence in the MWIR region, we measured the dispersion curve using several visible and short-wave IR lasers at room temperature. Results are plotted in Fig. 12. Dots are measured data at five discrete wavelengths and red curve represents the fitting results using following single-band model:

$$\Delta n = G \frac{\lambda^2 \lambda^{*2}}{\lambda^2 - \lambda^{*2}} \tag{6}$$

where G is a proportionality constant and λ^* is the mean resonance wavelength. Through fitting, we find $G = 3.37 \mu m^{-2}$ *and* $\lambda^* = 0.240 \mu m$. Based on these parameters, the Δn in the IR region can be extrapolated. As the wavelength increases, Δn decreases sharply and then plateaus in the MWIR

region. The birefringence of UCF-3 keeps relatively high (Δn~0.194) in the MWIR region. To achieve 2π phase change at λ=4μm, the required cell gap is 20.62μm. High Δn enables a thin cell gap to be used for achieving a certain phase change, which in turn leads to fast response time and high transmittance. We also measured the birefringence of UCF-1, and its Δn=0.17 at T=25°C and λ=633nm, which is much smaller than that of UCF-3 (Δn=0.22).

B. Viscosity

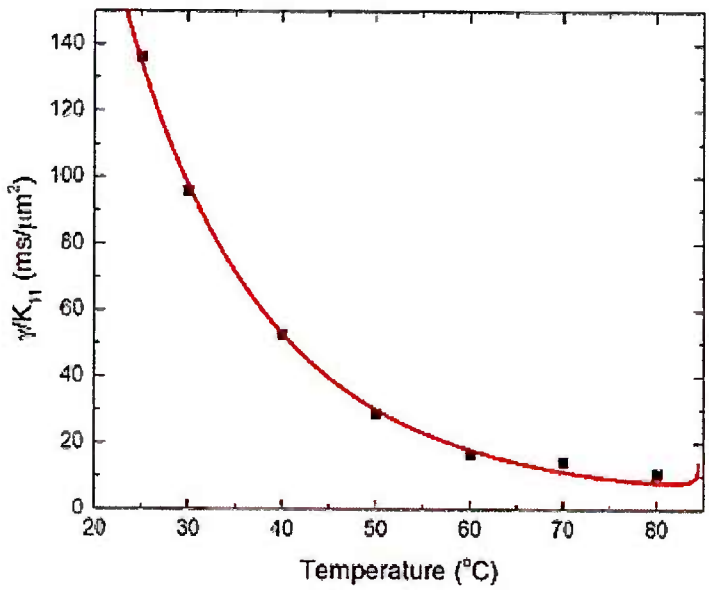

Fig. 13. Temperature dependent visco-elastic coefficient of UCF-3: dots are measured data and red line is fitting with Eq. (9). λ=633nm.

The visco-elastic coefficient (γ_1/K_{11}) was obtained by measuring the dynamic free relaxation time for a controlled phase change as:

$$\delta(t) = \delta_0 \exp\left(-\frac{2t}{\tau_0}\right), \tag{7}$$

$$\tau_0 = \frac{\gamma_1 d^2}{K_{11}\pi}, \tag{8}$$

here δ_0 is the total phase change, τ_0 is the relaxation time, γ_1 is rotational viscosity and K_{11} is the splay elastic constant. We plot visco-elastic coefficient for UCF-3 at different temperatures in Fig. 13, where dots are experimental data and red line is fitting curve with following equation:

$$\frac{\gamma_1}{K_{11}} = A\frac{\exp(E/K_B T)}{(1-T/T_C)}. \tag{9}$$

In Eq. (9), A is a proportional constant, E is the activation energy, T is the Kelvin temperature and K_B is the Boltzmann constant. For UCF-3, we find E=525meV. UCF-3 has a much larger visco-elastic coefficient (~140 ms/μm^2) than UCF-1 (~25 ms/μm^2) at room temperature. The possible explanations are: 1) the chlorine atom is heavier and bulkier than fluorine, and 2) the chloro compounds have longer alkyl chain. As the temperature increases, the visco-elastic coefficient decreases significantly. Besides, the estimated optical response time of UCF-3 is ~800ms. To

shorten the response time, a polymer network liquid crystal can be considered and the response time can be improved by 100x, but the tradeoff is increased operation voltage

C. IR transmittance for 2π phase change

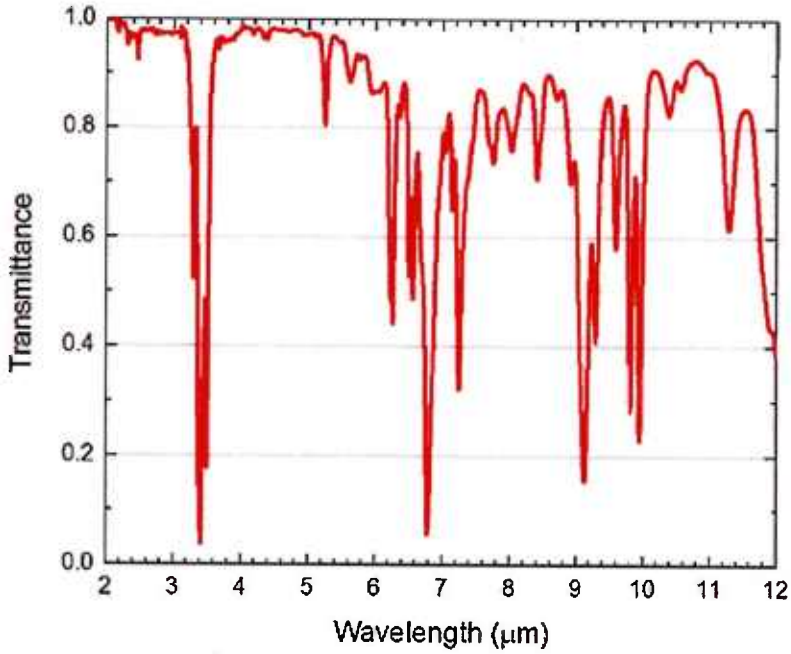

Fig. 14. Measured IR transmittance spectrum of UCF-3. Cell gap d=21μm.

To measure the IR transmittance, we filled UCF-3 to a LC cell with two sodium chloride (NaCl) substrates and measured the transmittance with a Perkin Elmer Spectrum One FTIR Spectrometer. The NaCl substrate is transparent from visible to 14μm and its refractive index ~1.5 is very close to that of the LC. To suppress the light scattering at room temperature, we spin-coated a thin PI layer (~80nm) on the inner surface of the NaCl substrates and gently rubbed the PI layer. Therefore, the LC molecules are aligned homogeneously. To achieve 2π phase change at λ=4μm, the required cell gap is 20.62μm. We fabricated an LC cell with a gap of d=21μm and Figure 14 depicts the measured transmittance of UCF-3 at room temperature from 2μm to 12μm. In the 3.8$\mu m \rightarrow$ 5μm region, the transmittance is ~98%. This is because the vibration peaks resulting from C-Cl bonds are shifted to beyond 12.5 μm and the overtone is outside the MWIR window as well. There is a strong absorption peak centered at 3.4μm resulting from the C-H stretching in the alkyl chain and aromatic rings, which are unavoidable since these C-H bonds are basic elements of organic compounds that exhibit a mesogenic phase. Besides, C-H bond vibrations contribute to the strong absorption at longer wavelength: (1) the C-H deformation in the alkyl chain and C-C skeletal stretching vibration peaks are located at 6~8μm; (2) the C-H in-plane deformation vibration peaks are at 8~10μm. On the other hand, in the case of a chlorine-substituted ring, the intensity of C-H in-plane bending vibrations is enhanced relative to other absorptions by as much as 3-4X. The absorption peak will degrade the transmittance of the off-resonance region as well. In order to achieve a 2π phase change at LWIR region, e.g. λ=10.6μm, the required cell gap is ~2x larger than

that at MWIR region and the transmittance at λ=10~11μm is expected to decrease to ~70%. This loss is too large, and other high Δn LC compounds should be considered, as will be discussed later.

D. Dielectric anisotropy

To determine dielectric anisotropy, we measured the capacitance of a homogenous cell and a homeotropic cell using an HP-4274 multi-frequency LCR meter. For UCF-3, we obtained $\Delta\varepsilon$ *=6.89 ($\varepsilon_{\parallel}$ =10.7, $\varepsilon_{\perp}$ =3.84)* at *23°C* and *f=1 kHz*. This medium $\Delta\varepsilon$ results from the modest C-Cl dipole group. UCF-1 aligns well in a homogeneous cell, but not so well in a homeotropic cell. Therefore, we can only estimate its $\Delta\varepsilon$ value through the measured threshold voltage ($3.4V_{rms}$) from a homogeneous cell. The estimated $\Delta\varepsilon$ is about 4. This small $\Delta\varepsilon$ value can be easily understood because some compounds listed in Table 3 have dipoles on both terminal groups. As a result, their dipole moments cancel each other.

3.5 Polymer network liquid crystal (PNLC) at MWIR

3.5.1 High birefringence liquid crystal host

First, we studied a commercial high birefringence LC mixture with Δn= 0.53 at λ=514nm and γ_1/K_{11}=17.0ms/μm^2 at room temperature. By measuring its birefringence at different wavelength, we can extrapolate its birefringence in the mid-wave infrared region as Δn=0.35 at λ=4μm. If an LC cell with gap d=12μm was employed to satisfy 2π phase change, the response time is 125ms. Moreover, to obtain super high birefringence, this mixture mainly contains compounds with –NCS group, it results in large and broad absorption band in the 4.5~5.5μm region. In the off-resonance region, the transmittance is only 95% with d=12μm.

Table 4. Chemical structures and properties of the cyano-terphenyl compounds studied, where Cr stands for crystalline, N for nematic, and I for isotropic Phase.

No.	Structure	PTT(°C)
1	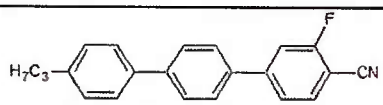	Cr 108.7 N 198.8 Iso
2		Cr 86.1 N 182.6 Iso
3	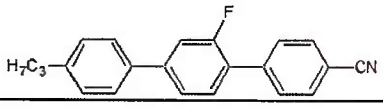	Cr 91.3 N 208.1 Iso
4	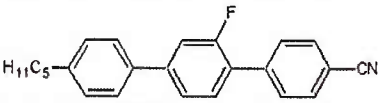	Cr 92.7 N 190.9 Iso

Table 4 lists four kinds of cyano-terphenyl compounds we prepared. Although –CN group has a very strong absorption peak at ~4.45μm, its bandwidth is relatively narrow. It elongates the conjugation length of the LC molecule and hence helps to increase the birefringence. The phase sequence and heating enthalpy of different compounds were measured using Differential Scanning

Calorimeter (DSC). As shown in Table 4, these compounds exhibit a relatively high melting point (T_{mp}). To lower T_{mp}, we formulated a eutectic mixture using these four compounds. The T_{mp} of this quaternary mixture is decreased to 36.3 °C. To lower the melting point further, we mixed 35 wt% UCF-2 into the cyano-terphenyl host. The resultant melting point of this mixture (UCF-4) is below -4°C, while the clearing point is 149.7°C. Its nematic range is quite wide.

A. Birefringence dispersion

We also measured the electro-optic properties of UCF-4. The methods are the same as that we used for UCF-3. Figure 15 shows the dispersion curve of UCF-4. The red line is the fitting curve with Eq. (6) with G=3.78μm^{-1} and λ^*=0.258μm. It saturates when the wavelength extends to IR region ($\lambda >> \lambda^*$). Thus it keeps high birefringence Δn=0.253 at λ=4μm, which helps to reduce the optical path.

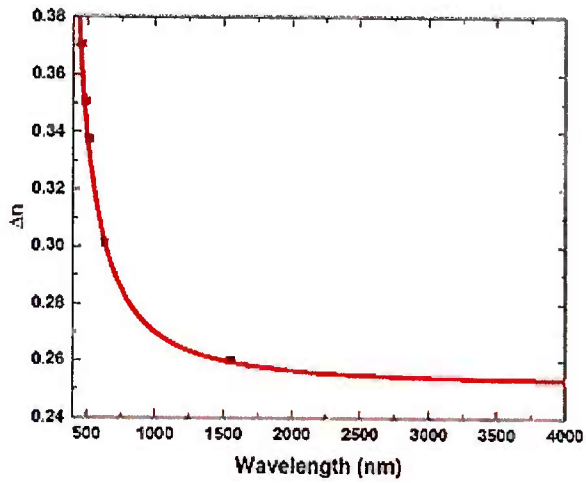

Fig. 15. Birefringence dispersion of UCF-4 at room temperature: dots are measured data and solid line is fitting with Eq. (6)

B. IR transmittance for 2π phase change

Using UCF-4, the required cell gap for achieving 2π phase change at λ=4μm is 24μm in transmissive mode. We fabricated an LC cell by employing two BaF_2 substrates with homogeneous alignment. The cell gap was controlled at 24μm by spacers. The transmittance spectrum was measured by FTIR at room temperature as well. Since LC molecules are aligned well with rubbing force, light scattering caused by LC directors is negligible. Figure 16 depicts the measured transmittance spectrum in the MWIR region. Though there is a strong absorption peak at λ=4.45μm due to –CN vibration, its transmittance is over 98% in the off-resonance region.

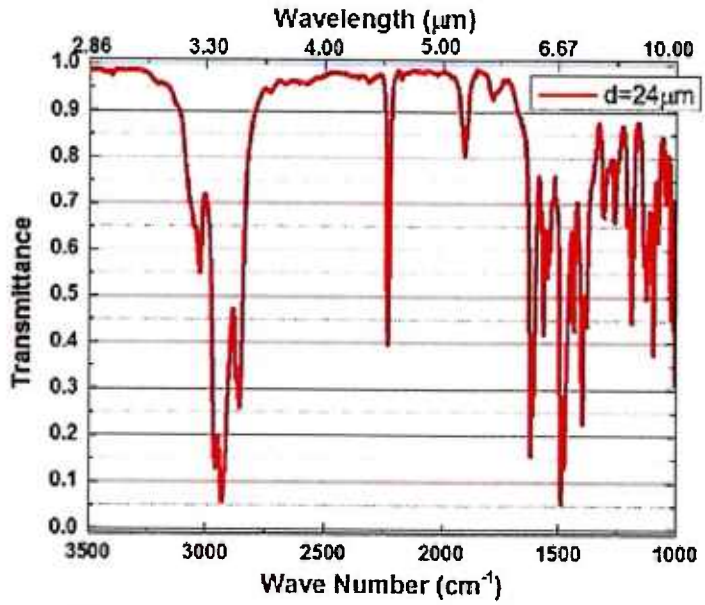

Fig. 16. Measured MWIR transmittance spectrum of UCF-4. Cell gap d=24 μm.

C. Visco-elastic constant coefficient

Figure17 depicts the temperature dependent visco-elastic constant of UCF-4. At room temperature (T=22°C), γ_1/K_{11}=113 ms/μm^2. The relatively large viscosity results from the rigid terphenyl cores, the cyano groups and chloro substitution. As the temperature increases, the visco-elastic constant decreases dramatically. The solid line in Fig.17 is theoretical fitting with Eq. (9). The fitting parameters are: A=1.38x10^{-7} ms/μm^2 and E=521.37meV. Thus, such large viscosity results in slow response time, which is not preferred in the beam steering applications. Therefore, polymer network liquid crystal is considered to achieve a fast response time.

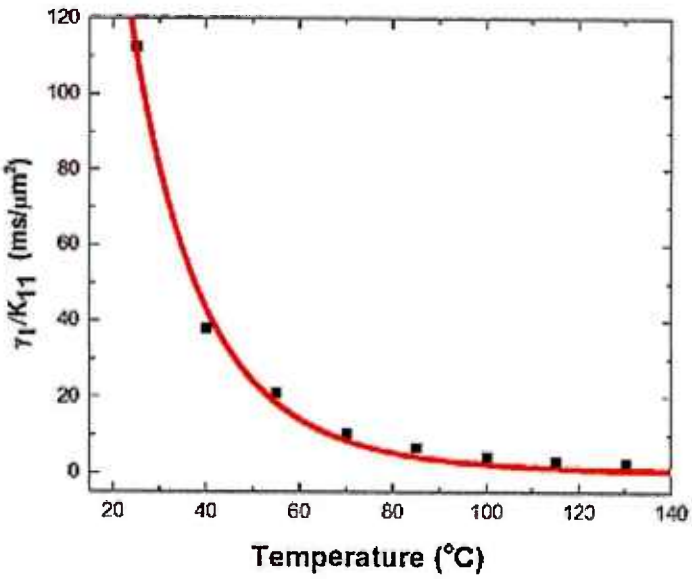

Fig. 17. Temperature dependent visco-elastic coefficient of UCF-4: dots are measured data and red line is fitting with Eq. (9). λ=633nm.

3.5.2 Performance of PNLC at MWIR

To fabricate PNLCs, we prepared a precursor by mixing 94.5wt% of UCF-4, with 5.0 wt% of RM257 and 0.5 wt% of photo-initiator. Here, we just use the monomer with mesogenic phase to maintain good alignment and obtain uniform phase profile. Then, the precursor was filled into homogeneous LC cells (indium tin oxide glass substrates). The cell gap was controlled at 11.8μm and the effective optical path is ~24μm in a reflective mode, which will satisfy the 2π phase change at λ=4μm. Thinner cell gap helps to reduce the operation voltage as well. In the UV curing process, we controlled the curing temperature at 0°C to obtain small domain size and fast response time is expected. Here, a UV light-emitting diode (LED) lamp (λ=385nm, Intensity is 300mW/cm^2) was employed and the exposure time for one hour. Since both terphenyl and cyano structure are stable under the UV exposure, It is suitable for UCF-4 employed as LC host in PNLC.

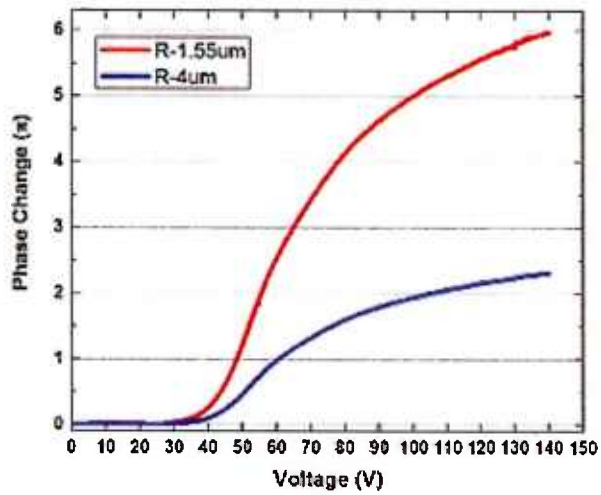

Fig. 18. Voltage-dependent phase change curves in a reflective mode at λ=1.5μm and λ=4μm.

To characterize the electro-optical properties of the PNLC cell, we measured its voltage-dependent transmittance (VT) with a laser beam at λ=1.55μm. Since here we use LC cell with glass substrate, which is not transparent at λ=4μm. The PNLC cell was sandwiched between two crossed polarizers, with the rubbing direction at 45° to the polarizer's transmission axis. We transferred VT curve into voltage-dependent phase curve as depicted in Fig.18. According to the dispersion curve shown in Fig. 15, birefringence becomes insensitive to the wavelength in the IR region. Therefore, we can transfer the voltage-dependent phase change curve from 1.55μm to 4μm confidently. Thus, the operation voltage ($V_{2\pi}$) is 105V at λ=4μm. Such a high operation voltage of PNLC is due to the strong anchoring force exerted by the polymer network.

However, it is the polymer network which helps decrease the response time. Figure19 shows the measured decay time of the PNLC cell. The initial biased voltage is 105V. Similar to measuring free relaxation time, the biased voltage was removed spontaneously at t=0, and the decay process initiated from 2π phase change at λ=4μm recorded. If we count the phase decay time from 100% to 10%, it is only 3.6ms, which is ~42X faster than that of the nematic LC mentioned previously.

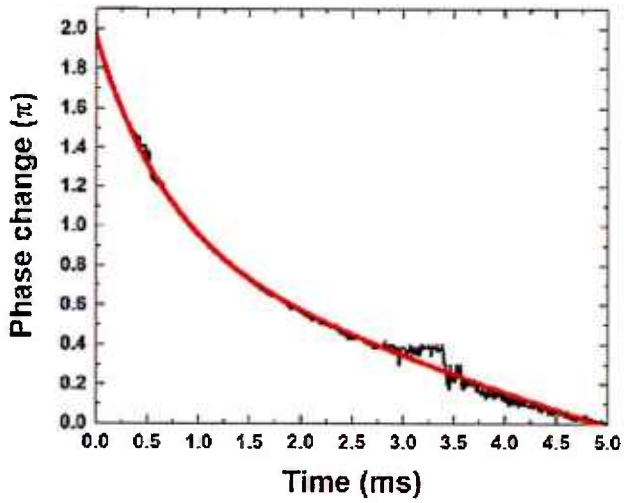

Fig. 19. Measured phase decay time of the PNLC sample. Black line is experimental data and red line is fitting with Eq. (7) and $\varphi_0=2\pi$.

3.6 High transmittance LC compounds at LWIR

3.6.1 High birefringence chlorinated LC

Eq. (1) describes the transmittance of an LC layer. Therefore, to minimize the absorption loss while keeping a required phase change ($\delta=2\pi d\Delta n/\lambda$) in the LWIR region ($\lambda=8\sim12\mu m$), two approaches can be considered: 1) To reduce the absorption coefficient α by substituting the C-H in-plane bending vibrations in the aromatic rings, and 2) to employ a high Δn LC to reduce the required cell gap or optical path length. A FoM is expressed in Eq. (2). Compound 13 in Table 3 possesses a high birefringence in the visible region ($\Delta n\sim0.35$ at $\lambda=633$nm) because the combination of the terphenyl core and the polar cyano group elongates the conjugation length. Based on the birefringence dispersion model, i.e. Eq. (6), Δn drops about 10~20% as the wavelength increases from the visible to IR. Here, we suppose $\Delta n\sim0.29$ at $\lambda=10.6\mu m$ and the required cell gap to get 2π phase change is $d=36.6\mu m$. We also include a commercial LC mixture E7 for comparison. Based on the birefringence dispersion of E7: $G=3.06\mu m^{-2}$ and $\lambda^*=0.250\mu m$, we find $\Delta n\sim0.19$ at $\lambda=10.6\mu m$. Thus, the required cell gap at this wavelength is $55.8\mu m$. To avoid scattering, we measured the transmittance of compound 13 in the isotropic phase at T~120°C. Figure 20 depicts the measured transmittance of compound 13 and mixture E7 in the LWIR. Compound 13 with higher birefringence and thinner cell gap shows a much higher transmittance than E7 at both $\lambda=8\sim9\mu m$ and $10\sim11\mu m$ regions. Some resonance bands of compound 13 are found at $\lambda=9\sim10\mu m$ because of C-H in-plane vibration resulting from tri-substituted and di-substituted phenyl rings. While the four components in E7 just have di-substituted phenyl rings. Although the CN group shows a relatively sharp and strong resonance peak at ~4.45μm, it does not degrade the transmittance in the LWIR region. Similar to UCF-3 for MWIR, we can also formulate eutectic mixtures consisting of homologs of compound 13 for LWIR applications.

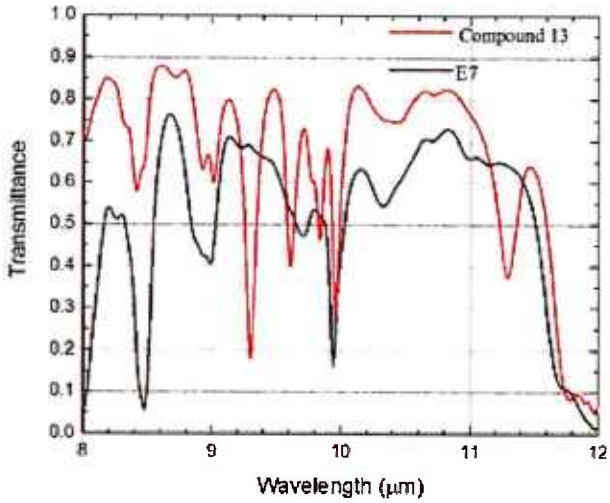

Fig. 20. Measured transmittance spectrum of compound 6 and mixture E7 in the LWIR region. The required cell gaps for compound 6 and mixture E7 are $37\mu m$ and $56\mu m$, respectively.

3.6.2 Partially deuterated LC compound

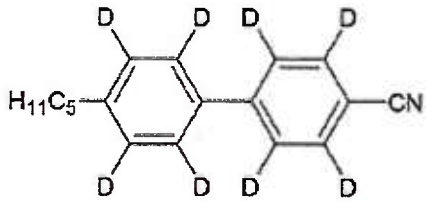

Fig. 21. The chemical structure of a partially deuterated 5CB we prepared for LWIR.

Substituting hydrogen with deuterium doubles the effective mass. Therefore, based on Eq. (3) the molecular vibration frequency would shift toward to a longer wavelength by $\sim\sqrt{2}$. There are several bending, symmetry and asymmetry deformations happening at 5~8μm, which are resulted from $-CH_2-$ and $-CH_3$ in the alkyl chain. After multiplying by a factor of $\sqrt{2}$, they would shift to the LWIR region (i.e. 8~12μm). On the other hand, the C-H in-plane and out-of-plane deformations of phenyl rings occur at 8~12μm. Thus, we should only replace the hydrogens in the phenyl rings to reduce absorption for LWIR band. We synthesized a partially deuterated 5CB, as shown in Fig. 21. The phase transition temperature was measured by DSC and it exhibits nematic phase from 7.0°C to 19.1°C, which is lower than that of non-deuterated 5CB (22.5~34.2°C). From gas chromatography our partially deuterated 5CB contains a couple of isomers with the same molecular weight and the chemical purity is ~95%. As a result, its phase transition temperature is lower than expected. We are in the process purifying our compound. The detailed synthesis processes will be discussed in Section 4.

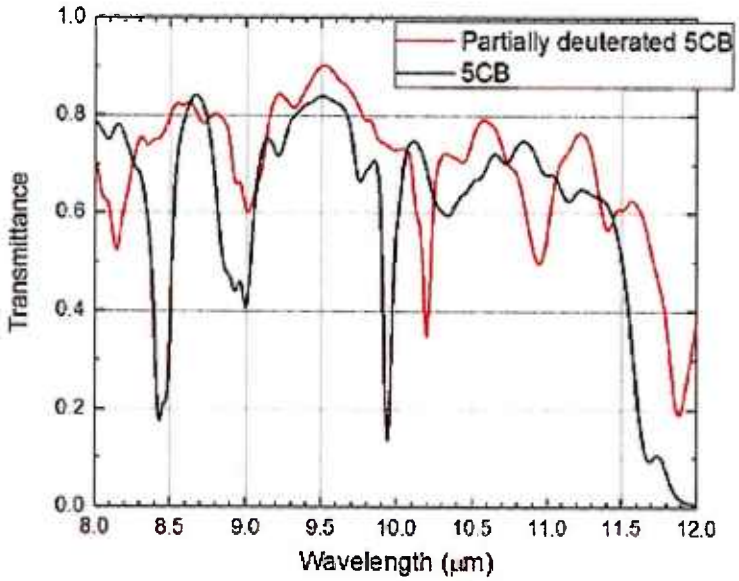

Fig. 22. The transmittance spectrum of partially deuterated 5CB and 5CB with cell gap ~55μm.

To measure the transmittance at LWIR, we fabricated an LC cell using two BaF_2 substrates. No PI layer and rubbing are applied because the sample shows isotropic phase at room temperature and no light scattering exists. The cell gap is controlled at ~55μm by spacers. The transmittance spectrums of both partially deuterated 5CB and non-deuterated 5CB are shown in Fig. 22. After deuteration, the overall transmittance gets higher and it achieves 90% at λ~9.5μm. The strong resonance peaks of 5CB at ~8.43μm, ~9.0μm and ~9.9μm resulting from C-H in-plane deformations are shifted outside LWIR region as we expected. The remaining resonance peaks at ~9.0μm and 10.9μm are due to the overtone of C-D out-of-plane deformation and fundamental in-plane deformation respectively. In addition, both C-C ring in-plane deformation and ring breathing vibration mode contribute to the resonance peak at ~10.2μm. To broaden the nematic temperature range, the compounds with higher purity and similar deuterated homologs could be considered to formulate a eutectic mixture.

4. Synthesis and Characterization of Materials

4.1 Introduction

The dominant and pervasive characteristic of the materials studies for this project involves the influence of the substitution of chlorine for hydrogen on the physical properties of highly conjugated oligophenyls. The most important and relevant properties of interest were the mesogenic activity, birefringence and absorption in critical areas of the infrared spectrum. Desired properties included nematic behavior at ambient temperature or as close to room temperature as possible, large birefringence in the IR and small absorption in selected MWIR and FWIR windows of device interest. Historically selective fluorination had been widely used to modify the phase behavior (temperature range) of liquid crystals with great success. However, when the requirements related to IR transparency are considered fluorination presents problems. As a result some alternative modification was sought and in this case that was examination of selective chlorination for control of phase behavior. Prior to this study some earlier literature described efforts to examine the role of chlorination on the phase behavior of liquid crystals but it was not as all clear if there was any general benefit and even less had been done concerning the relevant issues of transparency. This study now provides conclusive evidence that selective chlorination of oligophenyls is a very valuable tool to modify phase behavior (temperature range) and that the presence of chlorine is tolerable when specific transparency needs are considered.

A smaller component of the study (during the extension period) was an initiation of an examination of the selected deuteration of cyanobiphenyls and the influence on absorption in selected IR windows. While there are no conclusive results preliminary studies look very promising and need to be further pursued.

The materials prepared for this study are organized and discussed by class (and also thus pretty much chronologically). They include: 1) Chlorinated terphenyls; 2) Chlorinated Oligophenyls (Quaterphenyls and Quinquephenyls); 3) Chlorinated Cyclohexylterphenyls; 4) Ring Deuterated Cyanobiphenyls.

4.2 General synthesis comments

The materials examined in this study have much in common in that they are all oligophenyls but bear in addition a number and variety of substitutents. The deuterated materials differ somewhat and they are treated separately.

For the chlorinated materials fortunately there were a sufficient number of commercial precursors available that permitted the preparation of the chlorinated oligophenyls with reasonable ease. Future elaborations to further finesse these materials will likely require going beyond reliance on commercial precursors and will require the preparation of specific precursors possessing a number and location of chlorine atoms that are not currently commercially available.

For example, the following scheme (Fig. 23) for the preparation of ST04121 (shown in Table 5) is typical. In this case fortunately both components 1-bromo-2-chloro-4-iodobenzene and 4-n-pentylphenylboronic acids are commercially available. They are coupled by the Suzuki-Miyaura reaction to give the biphenyl shown. The success of this coupling reaction relies on the enhanced reactivity of the iodine vs. the bromine atom. In the subsequent step the remaining bromine atom is reacted with a different boronic acid (4-chlorophenylboronic acid) to provide the desired terphenyl. So, selected terphenyl isomers may be prepared taking advantage of manipulation of the sequence of reactions and the relative reactivity of the halogens present.

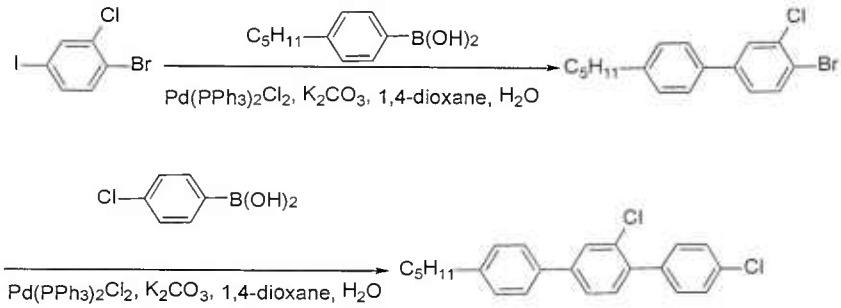

Fig. 23. The preparation scheme of ST 04121.

The same methodology applies to the synthesis of a representative quaterphenyl ST04139. The only important difference here is that the second boronic acid has two rings and a quaterphenyl (not a terphenyl) is the final product. Very generally the chlorine atoms are unreactive under typical Suzuki-Miyaura conditions we use and they are carried along without any interference.

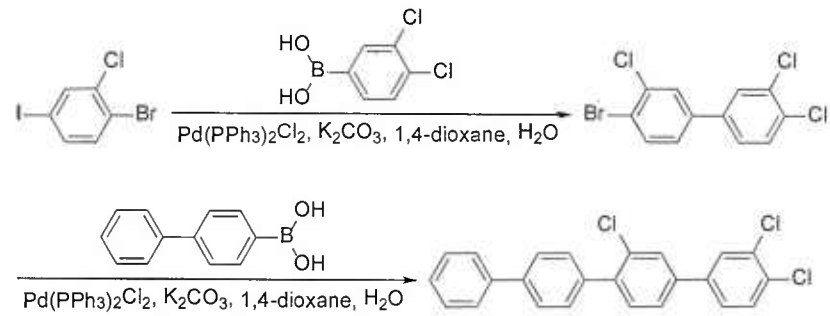

Fig. 24. The preparation scheme of ST 04139

In some special cases phenylboronic acids can be prepared from the respective halide via a lithium derivative and quenched with a trialkoxyboron derivative and then hydrolyzed to the boronic acid. The Suzuki-Miyaura reaction has been of critical importance in our preparation of the chlorine containing oligophenyls.

4.2.1 Chlorinated terphenyls

Table 5 shows some terphenyls prepared during the course of this study along with their phase behavior. Nematic phases (both thermotropic and monotropic) are quite pervasive amongst these chlorinated terphenyls. Some derivatives require further study (especially a subset which appear to be nematic at room temperature). Note all these materials possess an alkyl tail and at least a single chlorine atom. Some derivatives also contain fluorine and/or nitrile functionality which will influence absorption and thus utility in different IR windows.

Table 5. Chemical structures and properties of the terphenyls prepared, where Cr stands for crystalline, N for nematic, and Iso for isotropic phase.

Notebook number	Structure	Phase transition
ST 04 095	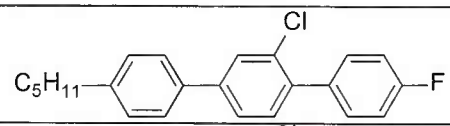	Cr 48.3 (N 30.1) Iso
ST 04 108	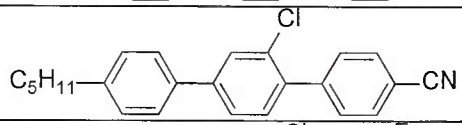	Cr 72 N 98 Iso
ST 04 107	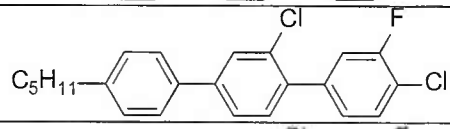	Cr 51°C N (6.1 °C) Iso
ST 04 113	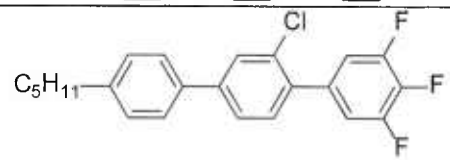	Nematic at room temperature
ST 04 114	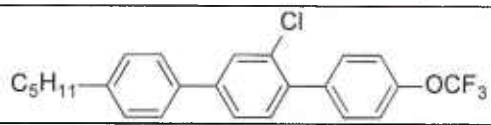	Nematic at room temperature
ST 04 120	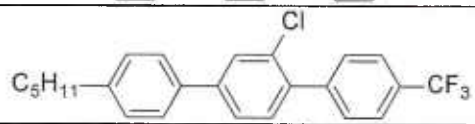	Cr 50 I
ST 04 121	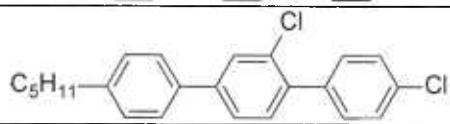	Cr 71 (N 65) I
ST 04 122	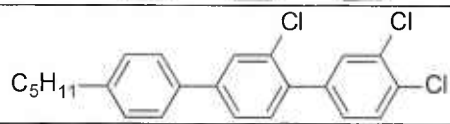	Nematic at room temperature
ST 04 128	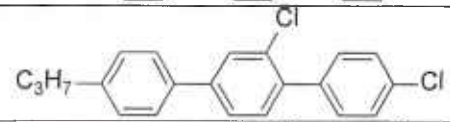	Cr 95 (N 68)I
ST 04 129	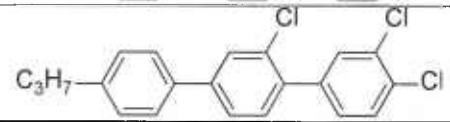	Nematic at room temperature

4.2.2 Chlorinated oligophenyls (quaterphenyls and quinquephenyls)

The alkyl tails in liquid crystals contribute to the absorption in the midwave infrared region to a large extent. The cyano group, aside from rendering excellent dipolar properties in the liquid crystal molecule is also responsible for absorption in the MWIR region. The C-H in-plane deformation in the phenyl rings also contribute to the absorption in the aforesaid region.

To mitigate the absorption loss due to the numerous C-H bonds in alkyl tails, the shortest possible alkyl tail should be used, although the best solution would be to design liquid crystals completely devoid of any alkyl tails. But exclusion of alkyl tails from the molecule design

generally elevates the melting point and reduces the flexibility of the molecule and thus reducing the liquid crystal phase stability or completely eliminating any liquid crystal phase. Some C-H bonds in the phenyl rings can be replaced by C-F or C-Cl bonds to reduce the absorption due to in-plane deformation. The absorption bands due to this deformation (skeletal vibrations involving C-C stretching in the ring) appears around 1600-1585 cm^{-1} and 1500-1400 cm^{-1}. When some hydrogens are replaced by Cl or F, the resultant mass of the oscillator increases, thus decreasing the frequency. The number and location of the halogens substituting for hydrogen must be carefully controlled. For example, the introduction of a significant number of fluorine atoms often leads to smectic phases in lieu of a nematic phase. In place of CN, NCS and other polar groups that absorb in the MWIR region, Cl or F can be used as they can insert a significant dipole moment without the undesirable absorption in the MWIR region.

The shortest known oligophenyl exhibiting mesogenic activity is *p*-quinquephenyl. But it has a very high transition temperature (Cr 388 N 420 I). The melting point becomes higher with additional benzene rings in the para position. Due to the insufficient aspect ratio, *p*-quaterphenyl is not mesogenic. It is also known that p-quaterphenyl itself has a very high clearing point[2] (322°C) due to very efficient molecular packing. If a para substituent is attached to quaterphenyl the aspect ratio may reach the critical value required for mesogenicity. All things considered, the best solution that we conceptualized for the design of liquid crystals for use in infrared applications was to use molecules with long conjugation without any alkyl tail and Cl as the polar group. The choice of Cl as the polar group is justified as it inserts significant dipole moment and does not contribute to the absorption in the MWIR region. Some *p*-quaterphenyls with *n*-pentyl tails that are laterally substituted with –Cl and $-CH_3$ and –NCS as polar head group are known to be nematic liquid crystals below 150°C. To lower the clearing point and render the molecule useful for any practical application the molecular packing needs to be disrupted by reducing the ring coplanarity and changing the intermolecular interactions of the quaterphenyl molecules in the crystal. For this purpose lateral substitution is often effective and the chlorine atom has been tried earlier as lateral substituent in liquid crystals.

With chlorinated quaterphenyls initial questions that need to be addressed include how many chlorines are productive and what will be the most effective placement for them in the molecule. To answer these questions, we have initiated a synthesis of some of the more readily available isomers. In particular, we have synthesized all the five unique monochloroquaterphenyls and compared their physical properties. The phase transitions of all the monochloroquaterphenyls are listed in Table 6

Table 6. Chemical structures and properties of monochloroquaterphenyl isomers.

Structure	Phase transition
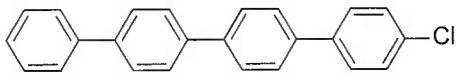	**(1)** 4-Cl Cr 334 N 348 I
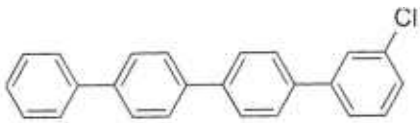	**(2)** 3-Cl Cr 242 SmX 255 I
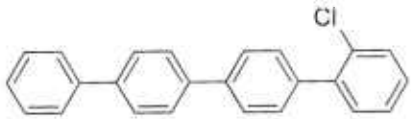	**(3)** 2-Cl Cr 175 I
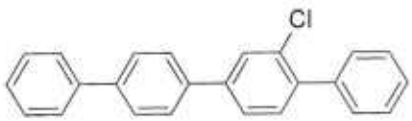	**(4)** 2'-Cl Cr 164 I
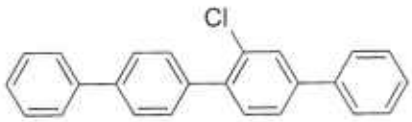	**(5)** 3'-Cl Cr 226 I

From Table 7 it is clear that the introduction of a single chlorine atom into *p*-quaterphenyl has a profound influence. First of all, in the case of introduction of chlorine in the para and meta position on the terminal ring (structures **1** and **2** respectively) a liquid crystal phase results (while in comparison the parent quaterphenyl has no liquid crystal phase). This is probably due to the fact that the specific placement of the chlorine atom in these two materials increases the aspect ratio[9] in a way that gives rise to long range order and changes the intricate interplay of intermolecular interactions-thus making them mesogenic. It can also be observed that the structures where the chlorine atom exerts the maximum disruption of ring coplanarity (structures 3, 4 and 5) undergo the most drastic reduction in the melting point compared to p-quaterphenyl (melting point 322°C[8]), although these molecules are not mesogenic. Combining these two structural aspects, it can be hypothesized that mesogenicity can be observed in a quaterphenyl within a manageable temperature range if we embellish the lateral positions systematically with chlorine while also using the chlorine as an end group to enhance the aspect ratio.

Based upon this result with the monochlorinated quaterphenyl isomers, we studied the effect of increasing the number of chlorines on the phase behavior. The influence of introduction of two chlorine atoms was examined next, and in the first set of five dichlorinated compounds no ring contained more than a single chlorine atom. Note that there are numerous other isomers in this

category that have not yet been prepared. The first five compounds examined were chosen solely on the basis of their synthetic accessibility.

Table 7. Phase transition temperatures of dichloroquaterphenyls
(only a single chlorine on any ring)

Structure	Phase transition
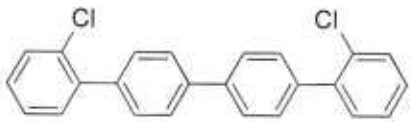	**(6)** Cr 168 I
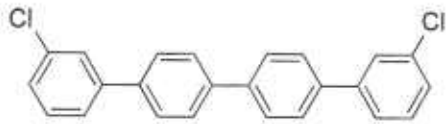	**(7)** Cr 220 I
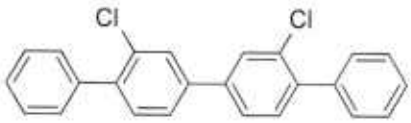	**(8)** Cr 148 I
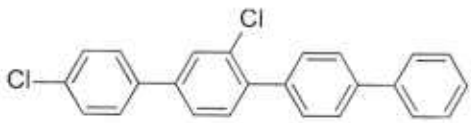	**(9)** Cr 217 N (181) I
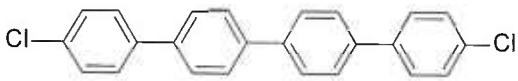	**(10)** Nematic at 321°C

Amongst these five dichlorinated compounds only the two examples (compounds **9** and **10**) having at least one para chlorine on a terminal ring was mesogenic. This finding further demonstrates the value of this structure feature to produce mesogenicity. Also, the two examples (compounds **6** and **8**) with the most internalized locations of the chlorine atoms have the most strongly perturbed phase behavior relative to the parent quaterphenyl. The synthesis and evaluation of other examples in this class is required in order to pursue any more discussion of the behavior here.

Following the synthesis of the dichlorinated isomers just three trichlorinated isomers were prepared. Here again these three are just a small fraction of the many trichlorinated isomers and they again were selected based only on their ease of synthesis. The three isomers are all gathered in Table 3 although if further isomers were prepared they might best ultimately be divided into more subsets. For example, compound **12** has no ring with more than one chlorine while compounds **11** and **13** might be distinguished as members of a separate set as each contains a ring with two chlorine atoms.

Table 8. Phase transition temperatures of chlorinated quaterphenyls.

Structure	Phase Transition
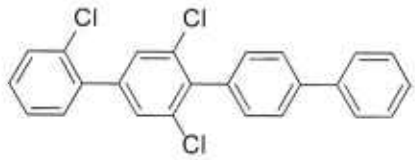	**(11)** Cr 163 I
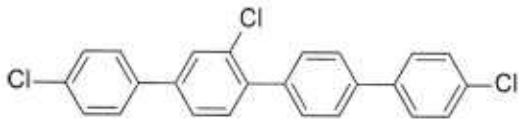	**(12)** Cr 167 N 319 I
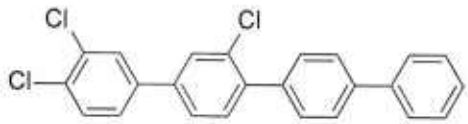	**(13)** Cr 272 N 285 I

In this case two of the three trichloroquaterphenyl isomers were mesogenic. The single nonmesogenic isomer is distinguished by the presence of two chlorine atoms appearing on a nonterminal ring and the absence of a chlorine atom on the para position of at least one terminal ring. It would be very interesting to look at additional trichloroquaterphenyls (e.g. 3,4,4'''-trichloroquaterphenyl).

Finally, three tetrachlorinated isomers, found in Table 4, were prepared. In materials **14** and **15** a pair of chlorines appear symmetrically on each of the terminal rings. Once again these two compounds were chosen only on the basis of their relative synthetic accessibility. Material **16** has the chlorines unsymmetrically distributed over the four benzene rings. It is anticipated that even more interesting properties might be found amongst the many other possible tetrachlorinated isomers.

Table 9. Phase transition temperatures of quaterphenyls with four or more chlorines.

Structure	Phase Transition
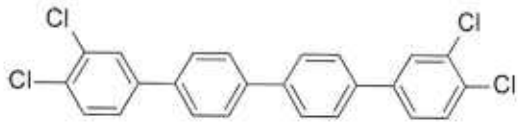	**(14)** Cr 200 N 221 I
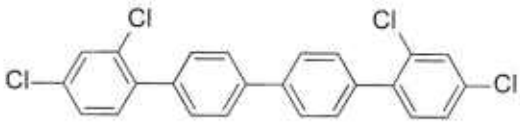	**(15)** Cr 226 N(180) I
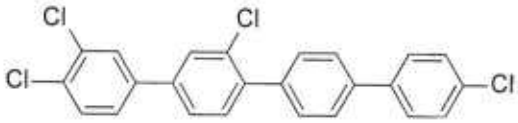	**(16)** Cr 135 N 161 I

Both of the symmetrical tetrachlorinated quaterphenyls examined have nematic phases (**14** enantiotropic and **15** monotropic). It would be especially interesting to see what the behavior of the less symmetric isomer 2,4,3''',4'''-tetrachloroquaterphenhyl would be.

The unsymmetrical tetrachlorinated quaterphenyl **16** exhibits a nematic phase at a much lower temperature. The melting point of this material is only 135°C (this is 187°C lower than parent quaterphenyl). With proper mixture formulation, the melting point can likely be lowered even more.

Finally, Fig. 25 the examination of the preparation of chlorinated quaterphenyls, a single monochloroquinquephenyl was prepared. As before, the lateral chlorination has drastic effect on the transition temperatures of quinquephenyl. The effect is demonstrated in the example of the 2'' monochlorination (melting reduction of 144 °C, clearing reduction of 116 °C).

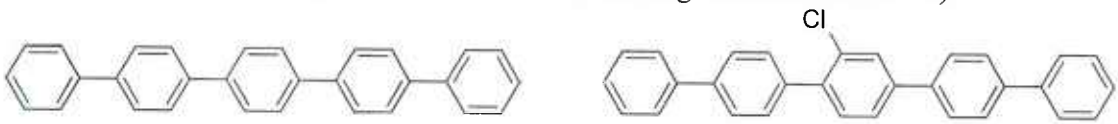

Phase transition: Cr 388 N 420 I

Phase transition: Cr 240 N 304 I

Fig. 25. The preparation scheme of chlorinated quaterphenyls.

Thus, we have studied the effect of lateral chlorination towards the development of liquid crystals transparent in the MWIR region. More materials need to be synthesized and mixtures formulated to make the materials useful for actual device application.

4.2.3 Chlorinated cyclohexylterphenyls

A series of compounds were made late in the project in which some of the chlorinated alkyl terphenyls were modified by the replacement of the n-alkyl tail by an n-alkylcyclohexyl tail. This modification led to some materials with much broader nematic phases. The synthesis modifications are summarized as below. The earlier studies had phenyl boronic acids of class 1 R=C_3H_7 or class 2 R = C_5H_{11}. The new materials had phenylboronic acids of class 4 R = C_3H_7cylclohexyl or class 5 C_5H_{11}cyclohexyl.

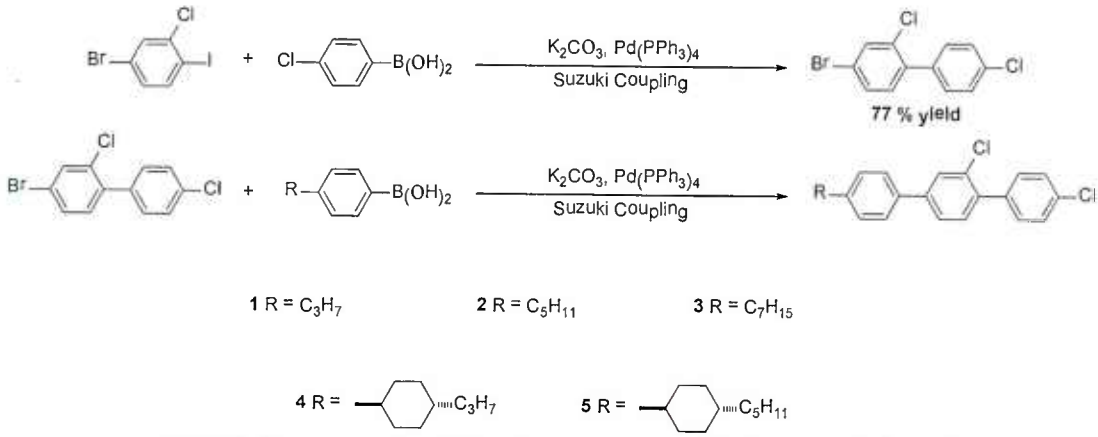

Fig. 26. The synthesis modifications of the chlorinated alkyl terphenyls.

Some class 3 materials with R = C_7H_{15} were also prepared to supplement the set of materials with shorter tails prepared in earlier studies. Notably this tail modification with a simple addition of a couple methylene units was far less effective than modification with the cyclohexane ring.

The requisite alkylcyclohexylphenylboronic acids were prepared from 1-bromo-4-(alkylcyclohexyl)benzenes which were very fortunately commercially available.

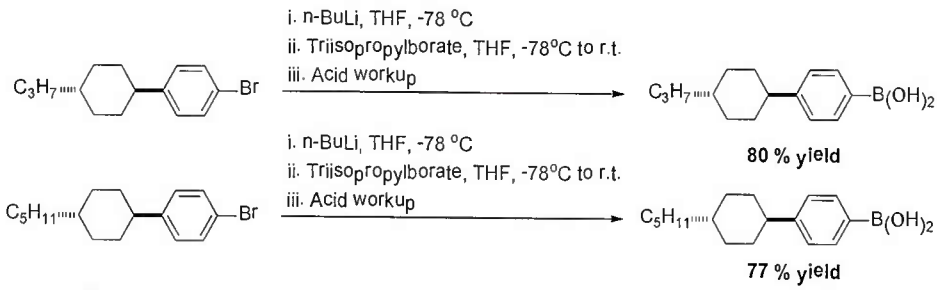

Fig. 27. The synthesis of the requisite alkylcyclohexylphenylboronic acids.

A typical synthesis of the a final alkylcyclohexylterphenyl is shown below for the specific case of the 2,2',4-trichlorinated compounds

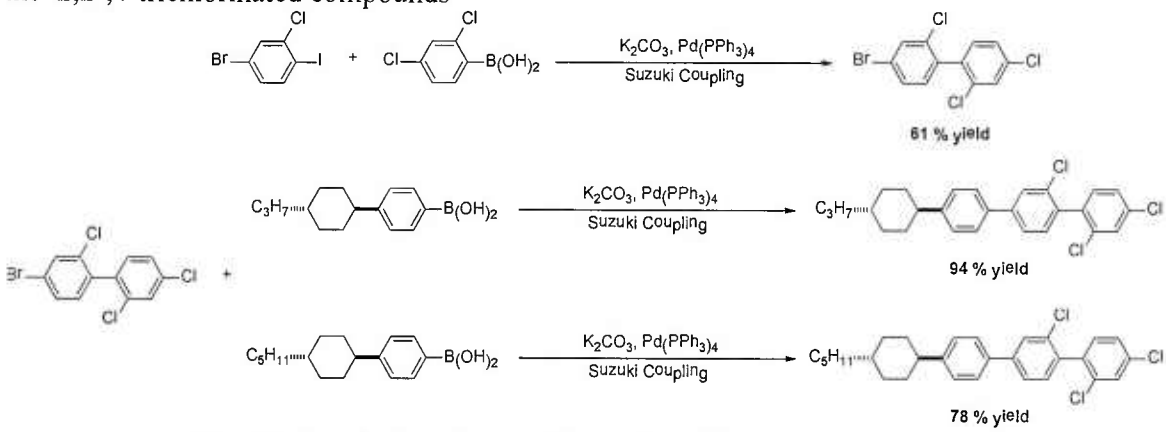

Fig. 28. A typical synthesis of the a final alkylcyclohexylterphenyl

Table 10. 2,2',4-trichlorinated alkylcyclohexylterphenyl compounds and their phase transitions:

Compound #.	Chemical structure	DSC (°C)
1 **ZL06089**	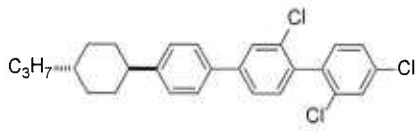	Cr 126 N 134 I 130 N 74 Cr
2 **ZL06091**	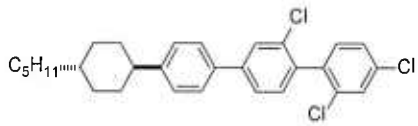	Cr 120 N 127 I 125 N 60 Cr

Table 11. 2',3,4-trichlorinated alkylcyclohexylterphenyl compounds and their phase transitions:

Compound #.	Chemical structure	DSC (°C)
1 **ZL06100**	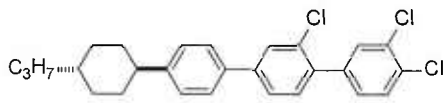	Cr 63 N 162 I 160 N
2 **ZL06097**	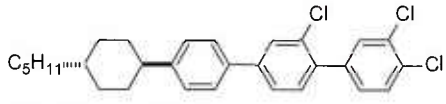	Cr 85 N 173 I 170 N

The dramatic influence of the replacement of the simple alkyl tail (1-3) below by the alkyl-cyclohexane ring (1-2) above becomes evident when we compare, for example, the two classes of materials. The four ring materials have nematic onsets that are somewhat higher in temperature when 2,2',4 substituted but the nematic range is also dramatically broader then the 2'4-dichlorinate materials. But the four ring 2',3,4-trichlorinated materials have nematic onsets which are comparable to the 2,4-dichlorinated materials. It is unlikely the optimal number and placement of chlorine atoms has been identified yet and further improvements in these critical properties are anticipated.

Table 12. Chemical structures and phase transition temperatures of chlorinated compounds

Compound #.	Chemical structure	T_m (°C)	T_c (°C)
1	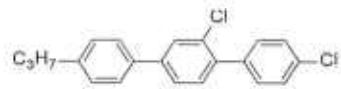	95	68
2	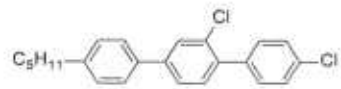	71	65
3	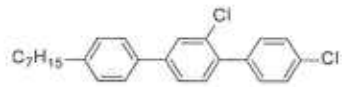	72	67

4.2.4 Ring deuterated cyano-biphenyls

Late in the project during the NCE period we undertook a study of deuterated cyano-biphenyl for a potential LWIR application. The specific goal here was to prepare 4-cyano-4'-n-pentylbiphenyl with full deuterium substitution on the aromatic rings and protium (regular hydrogen) on the tail. The initial synthetic scheme that was examined is shown below using nonlabeled biphenyl as the starting material. The process was effective but not perfect. We also went ahead and ran the same sequence on a sample of commercial perdeuterated biphenyl (Cambridge Isotopes).

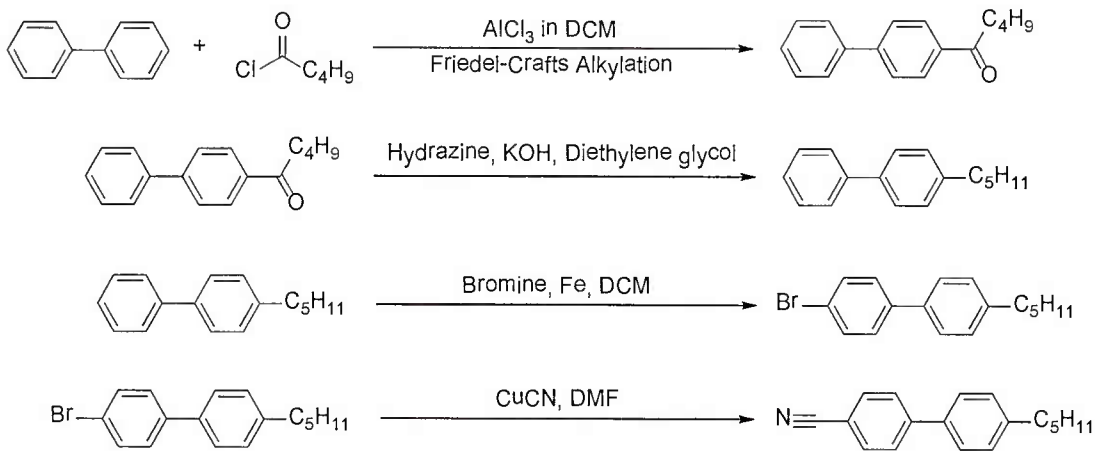

Fig. 29 The initial synthetic scheme for deuterated cyanobiphenyls

The chemical yields were reasonable throughout but the overall process appeared to have a weakness at the bromination stage. It appears that bromination of the pentylbiphenyl is not 100% at the para position and that at least two minor isomers are produced (e.g., bromination may have occurred in the alkylated ring as well). These isomers could not be separated and the isomer mixture was used in the cyanation stage, which produced a comparable set of cyanobiphenyl isomers which also cannot be separated. This mixture contained ~90% of the desired p-isomer (GC-MS) analysis but the presence of the small amount of the other isomers depressed and narrowed the nematic range of the ring deuterated sample. The proton NMR of this mixture indicates that the mixture is >90% deuterated in the ring (compared with the benzylic hydrogen content). Isomer content is not detected in the proton NMR (in part masked by the diminished proton content in the aromatic region).

A revised bromination process must be discovered which does not produce the isomer mix and/or some other intermediate after bromination must be utilized which is crystalline and will permit separation of the clean p-isomer prior to elaboration to the nitrile. For example, there are numerous methods now available to convert a benzoic acid to a nitrile cleanly and efficiently. If a carboxylic acid intermediate was involved in the process it could be purified readily by recrystallization to the pure p-isomer and in a separate step efficiently converted to the nitrile without isomerization and/or isotope scrambling.

Other reaction schemes by which this product might be obtained are feasible. For example, the deuteration might be done on the biphenyl with the alkyl tail present and perhaps even with the carboxylic acid and tail present. These approaches would serve as backup should a route using commercial d_{10}-biphenyl not suffice. In any case, there is nothing here that is not insurmountable.

5. Summary

We have developed several low loss nematic LC compounds and mixtures for MWIR and LWIR. For MWIR, the fluorinated and chlorinated compounds are synthesized. The fluorinated mixture UCF-1 shows a low-absorption window ($\alpha \approx 2.5 cm^{-1}$) at $\lambda \approx 3\mu m$. For the chlorinated LC mixtures, they show a low absorption window in the $\lambda = 4 \sim 5\mu m$ region. Besides, it possesses other attractive physical properties, such as wide nematic range (including room temperature), high birefringence at IR region, and modest positive dielectric anisotropy. In addition, we formulated a high birefringence LC mixture and its birefringence is 0.26 at $\lambda = 4\mu m$. The transmittance is higher than 98% in MWIR region. To achieve fast response time, we demonstrated a polymer network liquid crystal with 2π phase change at MWIR and response time less than 4 ms. For LWIR region, we have developed a chlorinated high birefringence LC compound to reduce the required optical path. Moreover, a phenyl ring-deuterated 5CB was synthesized to shift the resonance bands outside the LWIR region for improving transmittance.

6. Personnel involved in the project

In total, five (5) Ph.D. students are supported by this grant: 3 from UCF (Yuan Chen, Fenglin Peng, and Haiwei Chen) under the supervision of Prof. Shin-Tson Wu, and 2 from Kent State University (KSU) (Suvagata Tripathi and Zhe Li), under the supervision of Prof. Robert Twieg.

7. Publications

1. F. Peng, Y. Chen, S.T. Wu, S. Tripathi, and R. J. Twieg "Low loss liquid crystals for infrared applications," Liq. Cryst. **41**(11), 1545-1552 (2014).
2. F. Peng, Y. Chen, S. Tripathi, R. J. Twieg, and S. T. Wu, "A fast-response infrared phase modulator based on polymer network liquid crystal," Opt. Mater. Express **5**(2), 265-273 (2015).
3. F. Peng, Y. H. Lee, H. Chen, Z. Li, A. E. Bostwick, R. J. Twieg, and S. T. Wu, "Low absorption chlorinated liquid crystals for infrared applications," Opt. Mater. Express **5**(6), 1281-1288 (2015).
4. H. Chen, Z. Luo, R. Zhu, Q. Hong, and S. T. Wu, "Tuning the correlated color temperature of white LED with a guest-host liquid crystal," Opt. Express **23**(10), 13060-13068 (2015).

8. Presentations at conferences:

1. (Keynote) F. Peng, R. J. Twieg, and S. T. Wu, "Recent advances in IR liquid crystal spatial light modulators" SPIE Optics and Photonics, San Diego, California (August 23-27, 2015).
2. F. Peng, H. Chen, S. Tripathi, R. J. Twieg and S. T. Wu, "Fast-response IR spatial light modulators with a polymer network liquid crystal" SPIE Photonics West, San Francisco, California (Feb. 7-12, 2015).

9. Honors and Awards

Prof. Wu is a Charter Fellow of the National Academy of Inventors and among the first six inductees of the Florida Inventors Hall of Fame. He is a Fellow of the IEEE, OSA, SID, and SPIE, and the recipient of 2014 OSA Esther Hoffman Beller medal, 2011 SID Slottow-Owaki prize, 2010 OSA Joseph Fraunhofer award, 2008 SPIE G. G. Stokes award, and 2008 SID Jan Rajchman prize. Dr. Wu has co-authored 8 books and over 480 journal papers, and hold 83 U.S. patents. From 2012-2014, he served as OSA Publications Council Chair and Board of Directors, and from 2004 to 2008 he was the founding editor-in-chief of the IEEE/OSA Journal of Display Technology. Presently, Prof. Wu is serving as SID honors and awards committee chair and SPIE G.G. Stokes award committee member.